University College London
Department of Mathematics

# The fluid dynamics of chocolate fountains

Adam K. Townsend
adamtownsend.com

*Supervisor:* Dr Helen J. Wilson

M.Sci. Project in Mathematics

March 2012

# Contents

# Chapter 1

# Introduction

Chocolate fountains are a popular feature at special events. Melted chocolate is pumped over a series of domes and falls freely between them. In this project we model different fluid types over one such dome, and investigate how the fluid behaves in the different regions of the fountain: as it comes up the pipe (chapter 2), as it falls down the dome (chapter 3), how it leaves the dome, and how it falls freely (chapter 4). When fluid leaves the dome, it is observed that the fluid falls inwards rather than straight down and we offer an explanation and model for this.

Standard table chocolate fountains, such as in Figure 1.1, have two tiers and a small pool at the top for chocolate to gather before it travels down the edge and travels down the first dome. Chocolate is carried from the pool at the bottom of the fountain to the top by use of an Archimedes screw, but the existence of the pool at the top serves to remove all rotation in the fluid by the time it falls off. For this reason, and because axisymmetric pipe flows with pressure gradients are a nice introduction to the fluid models we will be discussing, we model the pipe as a vertical axisymmetric pipe with a constant pressure gradient. We then continue our mathematical considerations on the dome as the fluid approaches from the top. This model is shown in Figure 1.2.

Experimentally it was observed that in our fountain, the temperature of the chocolate remains constant (at 40 °C to within one degree) throughout its journey in the fountain so long as the fountain has been running for long enough (about thirty minutes). Wollny (2005) states that to within one degree, viscosity of chocolate should fluctuate between 5% and 10%. The much greater influence on viscosity is shear stress, which we consider in following chapters.

## 1.1 Modelling chocolate

When we consider different fluid models, what we are considering is the relationship (called the *constitutive* relation) between the stress and velocity gradient tensors


**Figure 1.1:** The chocolate fountain we are modelling in action.

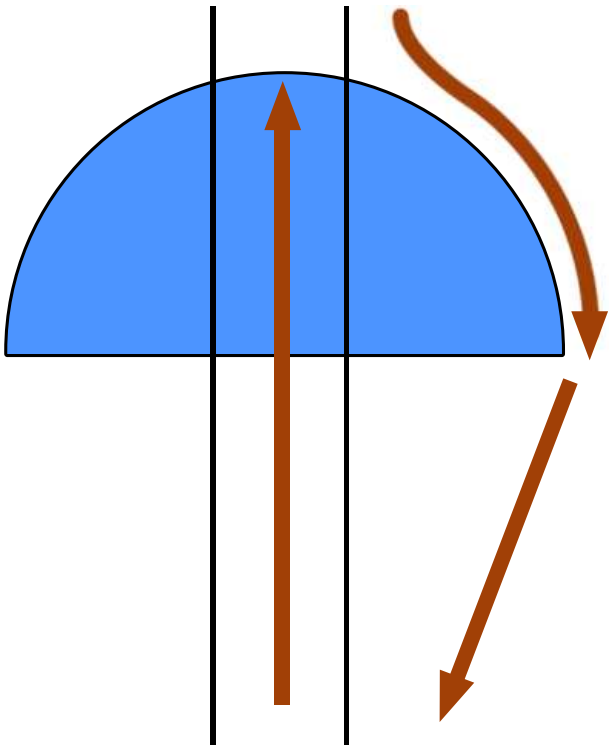

**Figure 1.2:** We model the chocolate fountain as a hemisphere atop a vertical cylindrical pipe, capturing the essence of the problem.

within the fluid. Formally, for a stress tensor $\boldsymbol{\sigma}$ and velocity vector $\mathbf{u}$,

$$\boldsymbol{\sigma} = \mathcal{F}\left(\boldsymbol{\nabla}\mathbf{u}, \boldsymbol{\nabla}\mathbf{u}|_{t<t_0}, \ldots\right),$$

where $\mathcal{F}$ is a functional which can take a multitude of arguments, possibly including: velocity gradient, temperature, electric fields, time, the scalar shear rate $\dot{\gamma}$ (defined below), and historical ($t < t_0$) values of all these quantities.

The shear rate tensor, $\dot{\boldsymbol{\gamma}}$, is defined as

$$\dot{\boldsymbol{\gamma}} = \boldsymbol{\nabla}\mathbf{u} + \boldsymbol{\nabla}\mathbf{u}^{\mathrm{T}}$$

and its scalar counterpart, $\dot{\gamma}$, is defined as

$$\dot{\gamma} = \left(\frac{1}{2}\boldsymbol{\nabla}\mathbf{u} : \boldsymbol{\nabla}\mathbf{u}\right)^{1/2} = \left(\frac{\dot{\gamma}_{ab}\dot{\gamma}_{ab}}{2}\right)^{1/2}, \tag{1.1}$$

where $\dot{\gamma}_{ij}$ is the $ij$th component of $\dot{\boldsymbol{\gamma}}$.

In a generalised Newtonian fluid, the functional $\mathcal{F}$ is a function $\mu$ of $\dot{\gamma}$ alone, and represents the viscosity,

$$\boldsymbol{\sigma} = \mu(\dot{\gamma})\dot{\boldsymbol{\gamma}},$$

and component-wise,

$$\sigma_{ij} = \mu(\dot{\gamma})\dot{\gamma}_{ij},$$

where $\sigma_{ij}$ is the $ij$th component of $\boldsymbol{\sigma}$. It is from this family of models that we shall choose to model chocolate in our chocolate fountain, since the temperature throughout the chocolate's path in the fountain does not change enough to warrant complicating the model.

In a simple shear flow in a channel of height $y$ and where the top of the channel is moving with speed $u$, as in Figure 1.3, the shear rate tensor is simply the scalar value

$$\dot{\boldsymbol{\gamma}} = \dot{\gamma} = \frac{\partial u}{\partial y}$$

and hence for a generalised Newtonian fluid,

$$\sigma = \mu(\dot{\gamma})\dot{\gamma} = f(\dot{\gamma}),$$

for some 'combined' function $f$. It is customary to introduce fluid models in this simple shear flow first, so this is how we shall proceed.

The simplest fluid model we shall be using is the **Newtonian model**, where there is proportionality between stress and strain rate,

$$\sigma = \mu\dot{\gamma},$$

and our viscosity $\mu$ is a constant. We shall be using a representative viscosity of chocolate at the sort of shear rates we are expecting (about $10\,\mathrm{s}^{-1}$) of $14\,\mathrm{Pa\,s}$. The viscosity of honey is $10\,\mathrm{Pa\,s}$ so this is a sensible value.

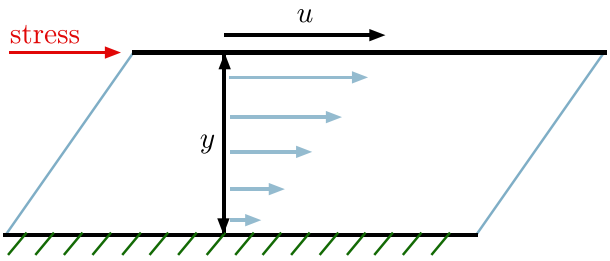


**Figure 1.3:** Shear flow in a 2D channel of height $y$ with a fixed base and a stress applied to the top, causing the top to move at a speed $u$.

In Casson (1959), N. Casson provides a model, originally designed for printing ink, which gives a constitutive equation of

$$\sqrt{\sigma} = \begin{cases} \sqrt{\mu_c \dot{\gamma}} + \sqrt{\sigma_y} & \text{if } \sigma \geq \sigma_y \\ \sqrt{\sigma_y} & \text{if } \sigma \leq \sigma_y \end{cases} \tag{1.2}$$

where $\mu_c$ is the Casson plastic viscosity, and $\sigma_y$ is the yield stress, given in pipe flow by

$$\sigma_y = \frac{r_c \sigma_w}{a} \tag{1.3}$$

where $r_c$ is the critical radial value (the value for which we expect plug flow), $\sigma_w$ is the stress upon the pipe wall, and $a$ is the radius of the pipe.

Typical values for chocolate, from industrial experiments (Mongia and Ziegler, 2000), are given in Table 2.1, where we explore this model more. This model, **Casson's model**, was recommended by the International Confectionery Association to model chocolate from 1973 until 2000, when Aeschlimann and Beckett (2000) found that at low shear rates, Casson's model does not fit the experimental rheology data well. As such it was difficult to find repeatability, and so interpolation data was recommended instead. (Sahin and Sumnu, 2006; Afoakwa et al., 2009).

Such interpolation data typically takes the form of a **power-law model**, where

$$\sigma = k\dot{\gamma}^n.$$

In component form, which we will use both in the pipe and on the dome in the following chapters, this is equivalent to

$$\sigma_{ij} = k\dot{\gamma}^{n-1}\dot{\gamma}_{ij} \tag{1.4}$$

where $\dot{\gamma}$ is that scalar shear rate defined in equation (1.1). Typical values for chocolate at 40 °C are, from industrial experiment (Radosasvljevic et al., 2000), $k = 65$ and $n = 0.3409$. Fluids with $n < 1$, as our chocolate is, are called *shear-thinning*, and include ceiling paint and tomato ketchup* among them. Fluids with $n > 1$ are called *shear-thickening*, of which a paste of cornflour and water is the best known. Of course, when $n = 1$, this model is equivalent to the Newtonian model. These relations are shown in Figure 1.4.

*Ketchup is actually a more special type of shear-thinning fluid, a Bingham fluid.

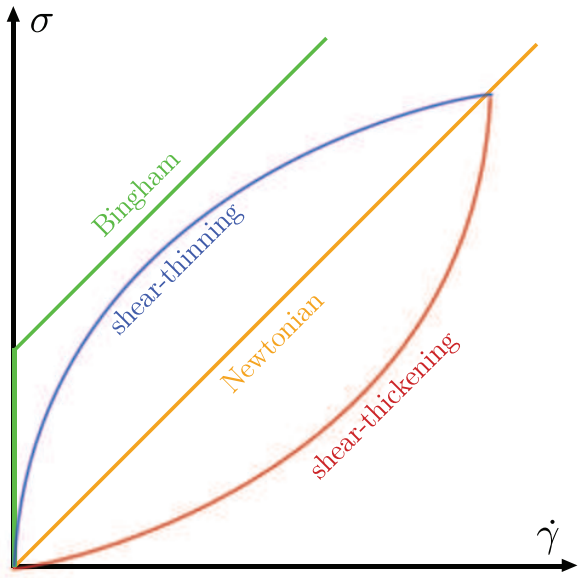


**Figure 1.4:** Graph of stress against rate of strain for a typical shear-thickening (dark red), Newtonian (orange), shear-thinning (blue) and Bingham fluid (green).

## 1.2 Typical values

At points in this project, we use experimental data to argue relative size of terms, or to compare expected result with what we observe in the chocolate fountain. Table 1.1 lists the typical values found from experiment, and relevant sources.

*Source: Radosasvljevic et al. (2000)

§Source: Keijbets et al. (2009). Experiments done with dark chocolate (50% cocoa), but this number is representative.

‡Source: Wichchukit et al. (2005). Experiments done with milk chocolate at 42 °C.

¶Source: Daubert et al. (1997). Experiments done with milk chocolate over a temperature range 25–60 °C.

| | | |
|---|---|---|
| Pipe radius | $a$ | $0.02\ \mathrm{m}$ |
| Dome radius | $R$ | $0.07\ \mathrm{m}$ |
| Density of chocolate[‡] | $\rho$ | $1270\ \mathrm{kg\,m^{-3}}$ |
| Surface tension of chocolate[§] | $\gamma_\mathrm{s}$ | $0.0226\ \mathrm{N\,m^{-1}}$ |
| Thermal diffusivity[¶] | $c$ | $6.32 \times 10^{-8}\ \mathrm{m^2\,s^{-1}}$ |
| Characteristic dome film thickness | $H$ | $0.001\ \mathrm{m}$ |
| Characteristic dome velocity | $U$ | $0.1\ \mathrm{m\,s^{-1}}$ |
| Typical dome leaving velocity | $u_0$ | $0.1\ \mathrm{m\,s^{-1}}$ |
| Characteristic sheet film thickness | $H$ | $0.0015\ \mathrm{m}$ |
| Gravitational acceleration | $g$ | $10\ \mathrm{m\,s^{-2}}$ |
| Drop height | $\ell$ | $0.07\ \mathrm{m}$ |
| Newtonian apparent viscosity | $\mu$ | $14\ \mathrm{Pa\,s}$ |
| Power-law flow consistency index[*] | $k$ | $64.728\ \mathrm{Pa\,s^n}$ |
| Power-law flow behaviour index[*] | $n$ | $0.3409$ |

**Table 1.1:** Table of values found experimentally

# Chapter 2

# The pipe

In a chocolate fountain, chocolate is heated at the bottom and is then transported to the top using an Archimedes spiral (and it is the rotating of the spiral which creates the noise associated with running it). Such spirals are difficult to model and since the rotation of the fluid makes observably minimal difference at the top of the fountain, we model the spiral as a vertical pipe with a constant pressure gradient. This choice of model also allows us to introduce relevant non-Newtonian fluid models within a geometry that is familiar and well-researched.

The radius of the pipe is $a$, and we will use cylindrical coordinates $(r, \theta, z)$ although the axisymmetric nature of the problem will lead us to expect no motion in the $\theta$ direction.

## 2.1 Newtonian, isothermal model

In our first model we model the chocolate as a viscous, incompressible Newtonian fluid, with constitutive equation

$$\boldsymbol{\sigma} = \mu\dot{\boldsymbol{\gamma}}$$

where $\mu$ is constant.

The Navier–Stokes equation for a viscous, incompressible Newtonian fluid is

$$\rho\frac{\mathrm{D}\mathbf{u}}{\mathrm{D}t} = -\nabla p + \mu\nabla^2\mathbf{u} + \mathbf{F} \tag{2.1}$$

where $\mathbf{u}$ is the velocity of the fluid, $\frac{\mathrm{D}}{\mathrm{D}t} = \frac{\partial}{\partial t} + \mathbf{u}\cdot\nabla$ is the material derivative, $\rho$ is the density of the fluid (assumed constant), $\mu$ is the viscosity of the fluid and $\mathbf{F}$ are external body forces (per unit volume).

Incompressibility gives us the continuity equation:

$$\nabla\cdot\mathbf{u} = 0.$$

In axisymmetric cylindrical polar coordinates, where the only external body force acting is gravity (downwards), these two equations are equivalent to the following system:

$$\rho\left(\frac{\partial u_r}{\partial t}+u_r\frac{\partial u_r}{\partial r}+u_z\frac{\partial u_r}{\partial z}\right)=-\frac{\partial p}{\partial r}+\mu\left[\frac{1}{r}\frac{\partial}{\partial r}\left(r\frac{\partial u_r}{\partial r}\right)+\frac{\partial^2 u_r}{\partial z^2}-\frac{u_r}{r^2}\right] \tag{2.2}$$

$$\rho\left(\frac{\partial u_z}{\partial t}+u_r\frac{\partial u_z}{\partial r}+u_z\frac{\partial u_z}{\partial z}\right)=-\frac{\partial p}{\partial z}+\mu\left[\frac{1}{r}\frac{\partial}{\partial r}\left(r\frac{\partial u_z}{\partial r}\right)+\frac{\partial^2 u_z}{\partial z^2}\right]-\rho g \tag{2.3}$$

$$\frac{1}{r}\frac{\partial}{\partial r}\left(ru_r\right)+\frac{\partial u_z}{\partial z}=0. \tag{2.4}$$

We expect steady flow, so we can say that

$$\frac{\partial u_r}{\partial t}=\frac{\partial u_z}{\partial t}=0.$$

Furthermore by symmetry we only expect flow in the $z$-direction, so we set

$$u_r=0 \quad \text{and} \quad u_z=u(r).$$

The three equations above then reduce to:

$$0=-\frac{\partial p}{\partial r} \tag{2.5}$$

$$0=-\frac{\partial p}{\partial z}+\mu\left[\frac{1}{r}\frac{\partial}{\partial r}\left(r\frac{\partial u}{\partial r}\right)\right]-\rho g \tag{2.6}$$

$$0=0. \tag{2.7}$$

Equation (2.5) tells us that $p=p(z,t)$ and equation (2.6) is the only thing left to solve.

We are assuming a constant pressure gradient

$$\frac{\partial p}{\partial z}=G=\text{const.}$$

with the boundary conditions

$$u(a)=0 \quad \text{no-slip condition} \tag{2.8}$$

$$\frac{\partial u}{\partial r}(0)=0 \quad \text{by symmetry} \tag{2.9}$$

If we let

$$H=-(G+\rho g),$$

the total pressure gradient including hydrostatic pressure, then equation (2.6) can be written

$$-H=\frac{\mu}{r}\frac{\partial}{\partial r}\left(r\frac{\partial u}{\partial r}\right)$$

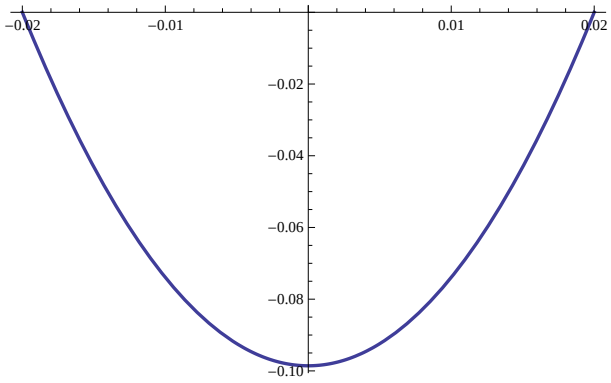


**Figure 2.1:** Velocity profile of a Newtonian fluid, given by (2.10). The pressure gradient $G$ is set to zero, hence we get downwards flow in the pipe. Constants are from Table 1.1

Rearranging and integrating once with respect to $r$,

$$\frac{-r^2 H}{2\mu} + C = r\frac{\partial u}{\partial r}.$$

Rearranging and integrating with respect to $r$ again,

$$\frac{-r^2 H}{4\mu} + C\ln r + D = u.$$

Boundary condition (2.8) tells us

$$D = \frac{a^2 H}{4\mu} - C\ln a$$

and boundary condition (2.9) gives $C = 0$ and so

$$u = \frac{a^2 H}{4\mu} - \frac{r^2 H}{4\mu}$$

and substituting in $H$ gives

$$u = (r^2 - a^2)\frac{G + \rho g}{4\mu}, \tag{2.10}$$

our velocity profile for a Newtonian fluid in a pipe with constant pressure head (Poiseuille flow). Note that we shouldn't be worried that $r^2 - a^2$ is mostly negative: in the absence of a pressure gradient $G$, we would, of course, expect fluid to fall *down* the tube, in the $-z$-direction. Figure 2.1 shows this velocity profile, in the absence of a pressure gradient, which is a parabola.

## 2.2 Power-law fluid

We consider a power-law fluid travelling up a vertical pipe. The Navier–Stokes equation for a general fluid is

$$\rho\frac{\mathrm{D}\mathbf{u}}{\mathrm{D}t} = -\nabla p + \nabla\cdot\boldsymbol{\sigma} + \mathbf{F} \tag{2.11}$$

(which reduces to (2.1) for a Newtonian fluid) where $\boldsymbol{\sigma}$ is the stress tensor (note that some authors include the pressure within their definition of the stress tensor). Expanded into cylindrical polar coordinates for an axisymmetric flow, where downwards gravity is the only external force, this is equivalent to

$$\rho\left(\frac{\partial u_r}{\partial t} + u_r\frac{\partial u_r}{\partial r} + u_z\frac{\partial u_r}{\partial z}\right) = -\frac{\partial p}{\partial r} - \left[\frac{1}{r}\frac{\partial}{\partial r}(r\sigma_{rr}) - \frac{\sigma_{\theta\theta}}{r} + \frac{\partial\sigma_{rz}}{\partial z}\right] \tag{2.12}$$

$$\rho\left(\frac{\partial u_z}{\partial t} + u_r\frac{\partial u_z}{\partial r} + u_z\frac{\partial u_z}{\partial z}\right) = -\frac{\partial p}{\partial z} - \left[\frac{1}{r}\frac{\partial}{\partial r}(r\sigma_{zr}) + \frac{\partial\sigma_{zz}}{\partial z}\right] - \rho g \tag{2.13}$$

$$\frac{1}{r}\frac{\partial}{\partial r}(ru_r) + \frac{\partial}{\partial z}(u_z) = 0. \tag{2.14}$$

Steady flow demands

$$\frac{\partial u_r}{\partial t} = \frac{\partial u_z}{\partial t} = 0$$

and by symmetry we expect flow only in the $z$-direction, so we set

$$u_r = 0 \quad \text{and} \quad u_z = u_z(r).$$

We now seek to find which components of stress become zero under these velocity assumptions. For a generalised Newtonian fluid, such as the power-law model we're using here, if a given component of $\dot{\boldsymbol{\gamma}}$ is zero, then the respective component of $\boldsymbol{\sigma}$ is too. For the power-law model, this is explicit in equation (1.4). In cylindrical coordinates, the components of rate of strain $\dot{\boldsymbol{\gamma}}$ for an incompressible fluid are given by

$$\begin{aligned}
\dot{\gamma}_{rr} &= 2\frac{\partial u_r}{\partial r}\\
\dot{\gamma}_{\theta\theta} &= 2\left(\frac{1}{r}\frac{\partial u_\theta}{\partial\theta} + \frac{u_r}{r}\right)\\
\dot{\gamma}_{zz} &= 2\frac{\partial u_z}{\partial z}\\
\dot{\gamma}_{r\theta} = \dot{\gamma}_{\theta r} &= r\frac{\partial}{\partial r}\left(\frac{u_\theta}{r}\right) + \frac{1}{r}\frac{\partial u_r}{\partial\theta}\\
\dot{\gamma}_{rz} = \dot{\gamma}_{zr} &= \frac{\partial u_z}{\partial r} + \frac{\partial u_r}{\partial z}\\
\dot{\gamma}_{\theta z} = \dot{\gamma}_{z\theta} &= \frac{\partial u_\theta}{\partial z} + \frac{1}{r}\frac{\partial u_z}{\partial\theta}.
\end{aligned} \tag{2.15}$$

Under the assumptions $u_\theta = u_r = 0$ and $u_z = u_z(r)$, the only non-zero component of $\dot{\boldsymbol{\gamma}}$ is $\dot{\gamma}_{rz}$ and so the only non-zero component of $\boldsymbol{\sigma}$ is $\sigma_{rz} = \sigma_{zr}$.

With this in mind then, equations (2.12)–(2.14) reduce to

$$0 = -\frac{\partial p}{\partial r} \tag{2.16}$$

$$0 = -\frac{\partial p}{\partial z} + \frac{1}{r}\frac{\partial}{\partial r}(r\sigma_{zr}) - \rho g \tag{2.17}$$

$$0 = 0. \tag{2.18}$$

We notate the steady pressure gradient thus,

$$\frac{\partial p}{\partial z} = G = \text{const.}$$

and for convenience we add the gravity term to form the pressure head, $H$,

$$H = -(G + \rho g).$$

We are then left to solve

$$\frac{\partial}{\partial r}(r\sigma_{zr}) = Hr$$

which after integration with respect to $r$ and rearranging gives

$$\sigma_{zr} = \frac{Hr}{2}. \tag{2.19}$$

Note that the constant of integration is set to zero by the boundary condition that $\sigma_{zr}(0) = 0$ by symmetry. Introducing the wall stress,

$$\sigma_{\mathrm{w}} = \frac{Ha}{2},$$

equation (2.19) is equivalent to

$$\sigma_{zr} = \sigma_{\mathrm{w}}\frac{r}{a}. \tag{2.20}$$

Equation (1.4) tells us

$$\sigma_{zr} = k\dot{\gamma}^{n-1}\dot{\gamma}_{zr},$$

and equation (2.15) tells us

$$\dot{\gamma} = \dot{\gamma}_{zr} = \frac{\mathrm{d}u_z}{\mathrm{d}r}, \tag{2.21}$$

where $\dot{\gamma}$ is our scalar shear rate, given by (1.1), and equal to $\dot{\gamma}_{zr}$ since it is the only non-zero component of strain rate.

Substituting this into equation (2.20) gives

$$k\left(\frac{\mathrm{d}u_z}{\mathrm{d}r}\right)^n = \sigma_{\mathrm{w}}\frac{r}{a},$$

which we can rearrange to find an expression for $\mathrm{d}u_z/\mathrm{d}r$,

$$\frac{\mathrm{d}u_z}{\mathrm{d}r} = \left(\frac{\sigma_{\mathrm{w}}}{ka}\right)^{1/n}(r)^{1/n}$$

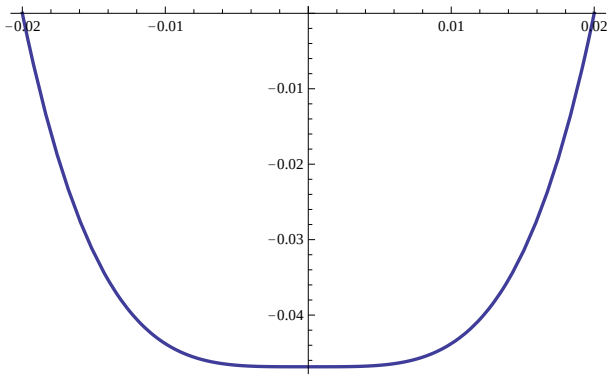


**Figure 2.2:** Velocity profile of a (shear-thinning) power-law fluid, given by (2.22). Constants are $G = 0$ (no pressure gradient, hence downward flow) and the rest from Table 1.1

and then integrating with respect to $r$ and noting the boundary condition $u_z(a) = 0$, gives

$$u_z = \left(\frac{\sigma_\mathrm{w}}{ka}\right)^{1/n} \frac{r^{1+1/n} - a^{1+1/n}}{1 + 1/n}. \tag{2.22}$$

In a Newtonian liquid, $k = \mu$ and $n = 1$ in equation (1.4) and substituting these values into (2.22) gives us

$$\begin{aligned} u_z &= \frac{\sigma_\mathrm{w}}{\mu a} \frac{r^2 - a^2}{2} \\ &= \frac{H}{2\mu} \frac{r^2 - a^2}{2} \\ &= (r^2 - a^2) \frac{G + \rho g}{4\mu} \end{aligned}$$

which is equivalent to equation (2.10).

Note that from our experimental data, the flow is slower with the power-law model: Figure 2.2 has been plotted with coefficients from the experimentally obtained data in Table 1.1, with the pressure gradient $G$ once again set to zero (hence we get downwards flow again). Maximum speed in the Newtonian model is $0.098\,\mathrm{ms}^{-1}$ and the maximum speed in the power-law model is $0.047\,\mathrm{ms}^{-1}$. The model used here has $n = \frac{1}{3} < 1$: i.e. chocolate is modelled as a shear-thinning fluid. The shape of the profile we see is somewhat similar to the parabola in the Newtonian case, but is considerably flatter at the centre: we see slower plug flow in the centre of the pipe, of width roughly a third of the diameter. Unlike in the Casson case which we shall see next, however, the flatness in the centre is not totally flat, $\partial u_z/\partial r \neq 0$: there is still some curvature.

## 2.3 Casson's model

In chapter 1, we introduced Casson's model, which gives a constitutive equation of

$$\sqrt{\sigma} = \begin{cases} \sqrt{\mu_{\mathrm{C}}\dot{\gamma}} + \sqrt{\sigma_{\mathrm{y}}} & \text{if } \sigma \geq \sigma_{\mathrm{y}} \\ \sqrt{\sigma_{\mathrm{y}}} & \text{if } \sigma \leq \sigma_{\mathrm{y}} \end{cases}$$

where $\mu_{\mathrm{C}}$ is the Casson plastic viscosity, and $\sigma_{\mathrm{y}}$ is the yield stress, given by

$$\sigma_{\mathrm{y}} = \frac{r_{\mathrm{c}}\sigma_{\mathrm{w}}}{a}.$$

Recall equation (2.20):

$$\sigma_{zr} = \sigma_{\mathrm{w}}\frac{r}{a}.$$

This time we square root this and substitute it into Casson's model, equation (1.2),

$$\sqrt{\sigma_{\mathrm{w}}\frac{r}{a}} = \sqrt{\mu_{\mathrm{C}}\dot{\gamma}} + \sqrt{\sigma_{\mathrm{y}}}, \tag{2.23}$$

for $\sigma_{zr} > \sigma_{\mathrm{y}}$. Solving for $\dot{\gamma}_{zr}$ gives

$$\dot{\gamma}_{zr} = \frac{\left(\sqrt{\sigma_{\mathrm{w}}\frac{r}{a}} - \sqrt{\sigma_{\mathrm{y}}}\right)^2}{\mu_{\mathrm{C}}},$$

or, substituting in equation (2.21),

$$\frac{\mathrm{d}u_z}{\mathrm{d}r} = \frac{\left(\sqrt{\sigma_{\mathrm{w}}\frac{r}{a}} - \sqrt{\sigma_{\mathrm{y}}}\right)^2}{\mu_{\mathrm{C}}}. \tag{2.24}$$

We can integrate this with respect to $r$ to find

$$u_z = -\frac{r\left(8a\sqrt{\frac{\sigma_{\mathrm{y}} r\sigma_{\mathrm{w}}}{a}} - 6a\sigma_{\mathrm{y}} - 3r\sigma_{\mathrm{w}}\right)}{6a\mu_{\mathrm{C}}} + c.$$

Substituting in equation (1.3) for $\sigma_{\mathrm{y}}$,

$$\begin{aligned} &= -\frac{8r^{3/2}r_{\mathrm{c}}^{1/2}\sigma_{\mathrm{w}} - 6rr_{\mathrm{c}}\sigma_{\mathrm{w}} - 3r^2\sigma_{\mathrm{w}}}{6a\mu_{\mathrm{C}}} + c \\ &= -\frac{\sigma_{\mathrm{w}}}{2a\mu_{\mathrm{C}}}\left(\frac{8}{3}r^{3/2}r_{\mathrm{c}}^{1/2} - 2rr_{\mathrm{c}} - r^2\right) + c, \end{aligned}$$

and using the no-slip boundary condition $u(a) = 0$ we find

$$u_z(r) = \begin{cases} \frac{\sigma_{\mathrm{w}}}{2a\mu_{\mathrm{C}}}\left(\frac{8}{3}\left(a^{3/2} - r^{3/2}\right)r_{\mathrm{c}}^{1/2} - 2(a-r)r_{\mathrm{c}} - (a^2 - r^2)\right) & \text{if } r_{\mathrm{c}} \leq r \leq a \\ u(r_{\mathrm{c}}) & \text{if } 0 \leq r_{\mathrm{c}} < r_{\mathrm{c}} \end{cases}. \tag{2.25}$$

| Percentage of coarse chocolate powder | $\sigma_y$ (Pa) | $\mu_C$ (Pa s) |
|---|---|---|
| 0 | 8.01 | 5.60 |
| 25 | 6.64 | 3.70 |
| 50 | 4.63 | 3.17 |
| 75 | 2.79 | 3.60 |
| 100 | 1.92 | 4.78 |

**Table 2.1:** Table of values found for $\sigma_y$ and $\mu_C$ by Mongia and Ziegler (2000). The different chocolate samples were formed with a combination of coarse and fine chocolate powders, the percentages of which are given here.

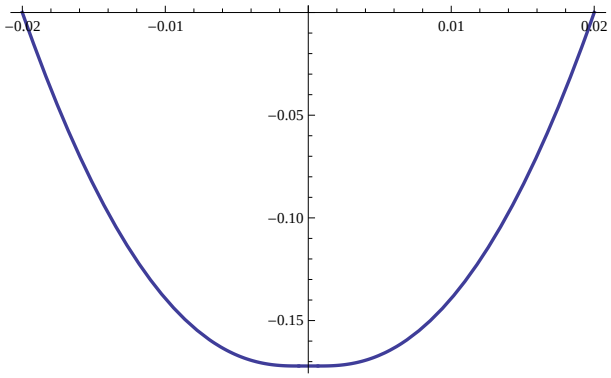


**Figure 2.3:** Velocity profile of a Casson fluid, given by (2.25). Constants are $G = 0$ (no upward pressure gradient, hence downwards flow), $\mu_C = 4.63$ (from Table 2.1), $r_c = 6.71 \times 10^{-4}$ and the rest from Table 1.1.

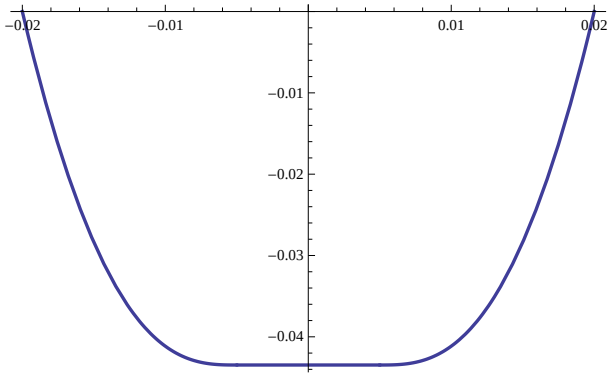


**Figure 2.4:** Velocity profile of a Casson fluid, with the same values as Figure 2.3, but with $r_c = 0.005$ to emphasise the properties of this fluid model.

Mongia and Ziegler (2000) give values for $\sigma_y$ and $\mu_C$, reproduced in Table 2.1. Using this table, we can find an estimate for $r_c$. If we use the value of $\sigma_y$ for the 50% sample, $G = 0$ and the values from Table 1.1 then

$$r_c = \frac{\sigma_y a}{\sigma_w} = \frac{4.63 \times 0.02}{1380 \times 10 \times 0.02/2} = 6.71 \times 10^{-4}$$

which is 3.4% of the radius of the pipe, so this is very small. This velocity profile has been illustrated in Figure 2.3, and again in Figure 2.4 but with an artificially larger critical radius of $r_c = 0.005$ to emphasise this property of Casson's fluid model. With small $r_c$, the profile looks very similar to the parabola seen in the Newtonian case, with a slight flatness at the centre. With larger $r_c$, it resembles much closer the power-law profile, with the plug flow in the centre. This time, however, the flatness seen in both large and small $r_c$ is truly flat, $\partial u_z/\partial r = 0$ in this area.

## 2.4 Generalised Newtonian fluid model

The procedures for finding velocity profiles in the preceding sections can be generalised easily (Wilkinson, 1960).

If we have a constitutive relation

$$\dot{\boldsymbol{\gamma}} = f(\boldsymbol{\sigma}), \tag{2.26}$$

for some function $f$, then for pipe flow this is equivalent to

$$\frac{\mathrm{d}u_z}{\mathrm{d}r} = f(\sigma_{zr}). \tag{2.27}$$

We can write the shear stress $\sigma_{zr}$ in terms of the wall shear stress, $\sigma_w$, as

$$\sigma_{zr} = \sigma_w \frac{r}{a}.$$

Substituting this into (2.27) gives

$$\frac{\mathrm{d}u_z}{\mathrm{d}r} = f\left(\sigma_w \frac{r}{a}\right),$$

and integrating with respect to $r$ with the no-slip boundary condition $u(a) = 0$ gives us our general velocity profile,

$$u_z(r) = \int_r^a f\left(\sigma_w \frac{r}{a}\right) \mathrm{d}r. \tag{2.28}$$

Of course the difficulty with this calculation is where the challenges lie, particularly since the constitutive equation represented in equation (2.26) is conventionally written in the inverse, i.e.

$$\boldsymbol{\sigma} = F(\dot{\boldsymbol{\gamma}}),$$

where $F = f^{-1}$.

# Chapter 3

# The dome

## 3.1 Isothermal Newtonian and power-law models

In this section we model movement of chocolate over the dome, being released at a constant rate from the very top of the dome. The resultant flow is described using lubrication theory. We model the dome as the top half of a sphere, but show that the analysis (and result) would work for any smooth shape, since the global curvature of the dome does not affect the motion of the fluid (mirroring other thin-film flows).

We set up spherical coordinates $(r, \theta, \phi)$ where $\theta$ is the inclination angle, $0 \leq \theta < \pi$, and $\phi$ is the azimuthal angle, $0 \leq \phi < 2\pi$. We label the radius of the sphere $R$ and the film thickness $h$. We expect axisymmetric flow so $h = h(\theta)$. This is summarised in Figure 3.1.

We use and compare two fluid models: the Newtonian model and the power-law model. We do not explore Casson's model in this geometry since the algebra would be considerably unwieldy, and we expect little difference between the Casson and power-law models. The differences in pipe flow between the Casson and power-law models, as seen in Figures 2.2 and 2.4, are very small anyway, and the difference between Newtonian and power-law flows (Figure 3.5) on the dome are in themselves slight, so we expect very little noticable difference between the Casson and power-law models on the dome.

For a general fluid, the Navier–Stokes equation can be written

$$\rho \frac{\mathrm{D}\mathbf{u}}{\mathrm{D}t} = -\nabla p + \nabla \cdot \boldsymbol{\sigma} + \mathbf{F} \tag{2.11}$$

where $\rho$ is our (constant) density, $\mathbf{u} = (u_r, u_\theta, u_\phi)$ is our velocity vector, $p$ is pressure, $\boldsymbol{\sigma}$ is our stress tensor, $\mathbf{F} = (F_r, F_\theta, F_\phi)$ are any external body forces (per unit volume), and $\mathrm{D}/\mathrm{D}t$ is the material derivative.

We expect a steady, axisymmetric flow, so we set $u_\phi = 0$ and $\partial/\partial\phi = 0$. The

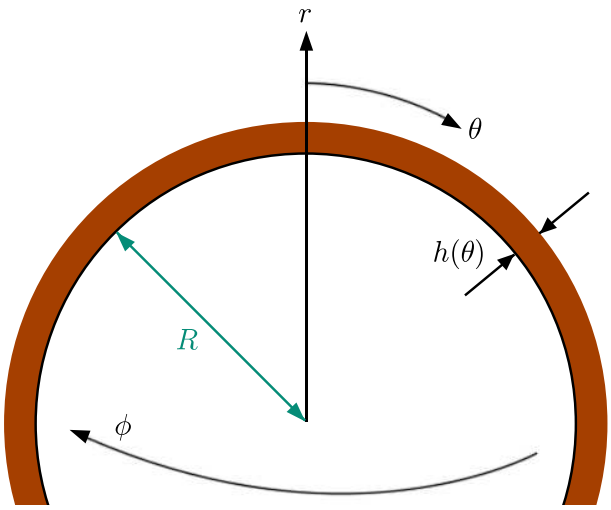


**Figure 3.1:** Coordinate setup for the dome problem

Navier–Stokes equations can then be written out in component form as

$$\rho\left[u_r\frac{\partial u_r}{\partial r}+\frac{u_\theta}{r}\frac{\partial u_r}{\partial \theta}-\frac{u_\theta^2}{r}\right] = -\frac{\partial p}{\partial r}-\left[\frac{1}{r^2}\frac{\partial}{\partial r}\left(r^2\sigma_{rr}\right)+\frac{1}{r\sin\theta}\frac{\partial}{\partial\theta}\left(\sigma_{r\theta}\sin\theta\right)-\frac{\sigma_{\theta\theta}+\sigma_{\phi\phi}}{r}\right]+F_r \tag{3.1}$$

$$\rho\left[u_r\frac{\partial u_\theta}{\partial r}+\frac{u_\theta}{r}\frac{\partial u_\theta}{\partial \theta}\right] = -\frac{1}{r}\frac{\partial p}{\partial\theta}-\left[\frac{1}{r^2}\frac{\partial}{\partial r}\left(r^2\sigma_{r\theta}\right)+\frac{1}{r\sin\theta}\frac{\partial}{\partial\theta}\left(\sigma_{\theta\theta}\sin\theta\right)+\frac{\sigma_{r\theta}}{r}-\frac{\sigma_{\phi\phi}\cot\theta}{r}\right]+F_\theta \tag{3.2}$$

$$0 = -\frac{1}{r\sin\theta}\frac{\partial p}{\partial\phi}-\left[\frac{1}{r^2}\frac{\partial}{\partial r}\left(r^2\sigma_{r\phi}\right)+\frac{1}{r}\frac{\partial\sigma_{\theta\phi}}{\partial\theta}+\frac{\sigma_{r\phi}}{r}+\frac{2\sigma_{\theta\phi}\cot\theta}{r}\right]+F_\phi \tag{3.3}$$

and our continuity equation is

$$0 = \frac{1}{r}\frac{\partial}{\partial r}\left(r^2u_r\right)+\frac{1}{\sin\theta}\frac{\partial}{\partial\theta}\left(u_\theta\sin\theta\right). \tag{3.4}$$

We seek the form of the $\boldsymbol{\sigma}$ components, and since in both models that we are using, the stress is a direct function of the shear rate $\dot{\boldsymbol{\gamma}}$, we write out the shear components for a general incompressible fluid, where we expect axisymmetric flow:

$$\begin{aligned}
\dot\gamma_{rr} &= 2\left[\frac{\partial u_r}{\partial r}\right]\\
\dot\gamma_{\theta\theta} &= 2\left[\frac{1}{r}\frac{\partial u_\theta}{\partial\theta}+\frac{u_r}{r}\right]\\
\dot\gamma_{\phi\phi} &= 2\left[\frac{u_r}{r}+\frac{u_\theta\cot\theta}{r}\right]\\
\dot\gamma_{r\theta}=\dot\gamma_{\theta r} &= \left[r\frac{\partial}{\partial r}\left(\frac{u_\theta}{r}\right)+\frac{1}{r}\frac{\partial u_r}{\partial\theta}\right]
\end{aligned} \tag{3.5}$$

$$\dot{\gamma}_{r\phi} = \dot{\gamma}_{\phi r} = 0$$
$$\dot{\gamma}_{\theta\phi} = \dot{\gamma}_{\phi\theta} = 0$$

Since our fluid models in component form are

$$\sigma_{ij} = \mu\dot{\gamma}_{ij}, \qquad \sigma_{ij} = k\dot{\gamma}^{n-1}\dot{\gamma}_{ij}$$

where $\dot{\gamma} = \sqrt{\dot{\gamma}_{ab}\dot{\gamma}_{ab}/2}$ (using Einstein summation convention), zero shear rate leads to zero stress component-wise. Hence the $\phi$-momentum equation (3.3) reduces to

$$0 = -\frac{1}{r\sin\theta}\frac{\partial p}{\partial \phi} + F_\phi. \tag{3.6}$$

We now introduce gravity as our only external force, hence

$$(F_r, F_\theta, F_\phi) = (-\rho g\cos\theta, \rho g\sin\theta, 0).$$

This reduces our $\phi$-momentum equation (3.6) to merely saying $p = p(r,\theta)$ (which we could have expected) and the $r$- and $\theta$-momentum equations (3.1)–(3.2) become

$$\begin{aligned}\rho&\left[u_r\frac{\partial u_r}{\partial r} + \frac{u_\theta}{r}\frac{\partial u_r}{\partial\theta} - \frac{u_\theta^2}{r}\right]\\ &= -\frac{\partial p}{\partial r} - \left[\frac{1}{r^2}\frac{\partial}{\partial r}\left(r^2\sigma_{rr}\right) + \frac{1}{r\sin\theta}\frac{\partial}{\partial\theta}\left(\sigma_{r\theta}\sin\theta\right) - \frac{\sigma_{\theta\theta}+\sigma_{\phi\phi}}{r}\right] - \rho g\cos\theta\end{aligned} \tag{3.7}$$

$$\begin{aligned}\rho&\left[u_r\frac{\partial u_\theta}{\partial r} + \frac{u_\theta}{r}\frac{\partial u_\theta}{\partial\theta}\right]\\ &= -\frac{1}{r}\frac{\partial p}{\partial\theta} - \left[\frac{1}{r^2}\frac{\partial}{\partial r}\left(r^2\sigma_{r\theta}\right) + \frac{1}{r\sin\theta}\frac{\partial}{\partial\theta}\left(\sigma_{\theta\theta}\sin\theta\right) + \frac{\sigma_{r\theta}}{r} - \frac{\sigma_{\phi\phi}\cot\theta}{r}\right] + \rho g\cos\theta.\end{aligned} \tag{3.8}$$

Since this system is too complicated to solve analytically, we have to introduce a scaling which will allow us to neglect comparatively small terms. We rescale our variables in the following way

$$\widehat{u}_\theta = \frac{u_\theta}{U}, \qquad \widehat{u}_r = \frac{u_r}{V}, \qquad \widehat{h} = \frac{h}{H}, \qquad \widehat{r} = \frac{r-R}{H}, \tag{3.9}$$

where hats denote scaled variables. $U$ and $V$ are characteristic speeds in the $\theta$- and $r$-direction respectively, $H$ is a characteristic film thickness, and $R$ is our already-established sphere radius. Note that our scaling for $r$ is unusual, but it emphasises the physical nature of the problem: the fluid occupies the space $R \le r \le R+h$, and our scaling converts this into $0 \le \widehat{r} \le h/H$, where $h/H \sim 1$.

What this means for our scaling is that

$$u_\theta \sim U, \qquad u_r \sim V, \qquad h \sim H, \qquad r \sim R, \qquad \partial/\partial r \sim 1/H. \tag{3.10}$$

The continuity equation (3.4) tells us how these characteristic values interact with each other. The equation is

$$0 = \frac{1}{r}\frac{\partial}{\partial r}\left(r^2 u_r\right) + \frac{1}{\sin\theta}\frac{\partial}{\partial\theta}\left(u_\theta\sin\theta\right).$$

and so

$$\frac{RV}{H} \sim U, \tag{3.11}$$

where we have substituted our scalings for our variables. Strictly, this comes from substituting our scaled variables (3.9) into the continuity equation, which would read

$$0 = \frac{1}{H\widehat{r} + R}\frac{1}{H}\frac{\partial}{\partial \widehat{r}}\left((R + H\widehat{r})^2 V u_r\right) + \frac{1}{\sin\theta}\frac{\partial}{\partial\theta}\left(U u_\theta \sin\theta\right),$$

and reading off the order of the terms. We will use the less strict approach in our forthcoming arguments, but strict treatment as shown here will give the same results. The important part of the equivalence (3.11) is that

$$V \sim \frac{UH}{R}$$

which is very small compared to $U$, since $H/R$ is small. Of course, this result is what we expect: flow is predominantly in the $\theta$-direction.

We intend, then, to look at how each term in equations (3.7)–(3.8) scales, but first we must look at how our stresses scale. Recalling that our constitutive relations in the Newtonian and power-law case are given by

$$\sigma_{ij} = \mu\dot{\gamma}_{ij}, \qquad \sigma_{ij} = k\dot{\gamma}^{n-1}\dot{\gamma}_{ij},$$

we look to see how our strains scale. Of course, finding this for the power-law case immediately finds this for the Newtonian case (by substituting $n = 1$ and $k = \mu$), so we concentrate on the power-law case.

Firstly, the scalar strain $\dot{\gamma} = \sqrt{\dot{\gamma}_{ab}\dot{\gamma}_{ab}/2}$ is given by

$$\begin{aligned}\dot{\gamma} = \Bigg\{\frac{1}{2}\Bigg[&\left(\frac{\partial u_r}{\partial r}\right)^2 + \left(\frac{1}{r}\right)^2\left(\frac{\partial u_\theta}{\partial\theta}\right)^2 + 2\left(\frac{u_r}{r}\right)^2 + \left(\frac{u_\theta\cot\theta}{r}\right)^2 \\ &+ \left(r\frac{\partial}{\partial r}\left(\frac{u_\theta}{r}\right)\right)^2 + \left(\frac{1}{r}\right)^2\left(\frac{\partial u_r}{\partial\theta}\right)^2\Bigg]\Bigg\}^{1/2}.\end{aligned} \tag{3.12}$$

Term-by-term, these terms scale as

$$\left[\frac{V^2}{H^2} + \frac{U^2}{R^2} + \frac{V^2}{R^2} + \frac{U^2}{R^2} + \frac{R^2}{H^2}\frac{U^2}{R^2} + \frac{U^2}{R^2}\right]^{1/2}$$

For the first term, $V/H \sim U/R$, and clearly the scalar strain scales predominantly as

$$\dot{\gamma} \sim \left(\frac{U^2}{H^2}\right)^{1/2} = \frac{U}{H}. \tag{3.13}$$

Now we look at the non-zero strain components again and see how they predominantly scale:

$$\begin{aligned}
\dot{\gamma}_{rr} &= 2\left[\frac{\partial u_r}{\partial r}\right] && \sim \frac{V}{H} \sim \frac{U}{R} \\
\dot{\gamma}_{\theta\theta} &= 2\left[\frac{1}{r}\frac{\partial u_\theta}{\partial \theta} + \frac{u_r}{r}\right] && \sim \frac{U}{R} \\
\dot{\gamma}_{\phi\phi} &= 2\left[\frac{u_r}{r} + \frac{u_\theta \cot\theta}{r}\right] && \sim \frac{U}{R} \\
\dot{\gamma}_{r\theta} = \dot{\gamma}_{\theta r} &= \left[r\frac{\partial}{\partial r}\left(\frac{u_\theta}{r}\right) + \frac{1}{r}\frac{\partial u_r}{\partial \theta}\right] && \sim \frac{U}{H}
\end{aligned}$$

Hence our non-zero stress components scale as

$$\begin{aligned}
\sigma_{rr} &\sim k\left(\frac{U}{H}\right)^{n-1}\frac{U}{R} = k\left(\frac{U}{H}\right)^{n}\frac{H}{R} \\
\sigma_{\theta\theta} &\sim k\left(\frac{U}{H}\right)^{n}\frac{H}{R} \\
\sigma_{\phi\phi} &\sim k\left(\frac{U}{H}\right)^{n}\frac{H}{R} \\
\sigma_{r\theta} = \sigma_{\theta r} &\sim k\left(\frac{U}{H}\right)^{n}.
\end{aligned}$$

So with this in mind we can now rewrite (3.7)–(3.8) and see how each term scales. So, to reiterate, our governing equations are

$$\begin{aligned}
&\rho\left[u_r\frac{\partial u_r}{\partial r} + \frac{u_\theta}{r}\frac{\partial u_r}{\partial \theta} - \frac{u_\theta^2}{r}\right] \\
&\quad = -\frac{\partial p}{\partial r} - \left[\frac{1}{r^2}\frac{\partial}{\partial r}\left(r^2\sigma_{rr}\right) + \frac{1}{r\sin\theta}\frac{\partial}{\partial \theta}\left(\sigma_{r\theta}\sin\theta\right) - \frac{\sigma_{\theta\theta}+\sigma_{\phi\phi}}{r}\right] - \rho g\cos\theta \quad (3.14) \\
&\rho\left[u_r\frac{\partial u_\theta}{\partial r} + \frac{u_\theta}{r}\frac{\partial u_\theta}{\partial \theta}\right] \\
&\quad = -\frac{1}{r}\frac{\partial p}{\partial \theta} - \left[\frac{1}{r^2}\frac{\partial}{\partial r}\left(r^2\sigma_{r\theta}\right) + \frac{1}{r\sin\theta}\frac{\partial}{\partial \theta}\left(\sigma_{\theta\theta}\sin\theta\right) + \frac{\sigma_{r\theta}}{r} - \frac{\sigma_{\phi\phi}\cot\theta}{r}\right] + \rho g\cos\theta. \\
&\qquad\qquad (3.15)
\end{aligned}$$

and these scale, term-by-term, as

$$\begin{aligned}
\rho\left[\frac{UV}{R} + \frac{UV}{R} - \frac{U^2}{R}\right] &= (?) - \left[\frac{k}{R}\left(\frac{U}{H}\right)^n + \frac{k}{R}\left(\frac{U}{H}\right)^n - \frac{Hk}{R^2}\left(\frac{U}{H}\right)^n + \frac{Hk}{R^2}\left(\frac{U}{H}\right)^n\right] + (?) \\
\rho\left[\frac{U^2}{R} + \frac{U^2}{R}\right] &= (?) - \left[\frac{k}{H}\left(\frac{U}{H}\right)^n + \frac{Hk}{R^2}\left(\frac{U}{H}\right)^n + \frac{k}{R}\left(\frac{U}{H}\right)^n - \frac{Hk}{R^2}\left(\frac{U}{H}\right)^n\right] + (?),
\end{aligned}$$

where we have marked by (?) those terms which we don't know the size of. Dividing

through by $\rho U^2/R$ gives a non-dimensional scaling,

$$\frac{V}{U} + \frac{V}{U} - 1 = (?) - \frac{1}{\mathrm{Re}}\left[\frac{R}{H} + \frac{R}{H} - 1 + 1\right] + (?) \tag{3.16}$$

$$1 + 1 = (?) - \frac{1}{\mathrm{Re}}\left[\left(\frac{R}{H}\right)^2 + 1 + \frac{R}{H} - 1\right] + (?), \tag{3.17}$$

where the Reynolds number Re is given by

$$\mathrm{Re} = \frac{\rho U R}{\mu} = \frac{\rho U R H^{n-1}}{k U^{n-1}} = \frac{\rho U^2 R}{Hk}\left(\frac{H}{U}\right)^n,$$

since $\mu = k\dot{\gamma}^{n-1}$ for a power-law fluid. Using the values from Table 1.1, we find for the Newtonian data, $\mathrm{Re} = 0.635$, and for the power-law data, $\mathrm{Re} = 2.86$. Both of these numbers are of the order we expect for slow, viscous fluid.

The dominant terms (over those that we know) in equation (3.16), which represents equation (3.14), are those of order $R/H$ since $R/H \gg 1$, $V/U \ll 1$ and the Reynolds number is of order 1. In equation (3.1), representing equation (3.15), the term which dominates is the $(R/H)^2$ term, since $(R/H)^2 \gg R/H \gg 1$ and again $\mathrm{Re} \sim 1$. This reduces our equations (3.14)–(3.15) to

$$0 = -\frac{\partial p}{\partial r} - \left[\frac{1}{r^2}\frac{\partial}{\partial r}\left(r^2\sigma_{rr}\right) + \frac{1}{r\sin\theta}\frac{\partial}{\partial\theta}\left(\sigma_{r\theta}\sin\theta\right)\right] - \rho g\cos\theta \tag{3.18}$$

$$\begin{aligned} 0 &= -\frac{1}{r}\frac{\partial p}{\partial\theta} - \frac{1}{r^2}\frac{\partial}{\partial r}\left(r^2\sigma_{r\theta}\right) + \rho g\cos\theta \\ &= -\frac{1}{r}\frac{\partial p}{\partial\theta} - \frac{\partial\sigma_{r\theta}}{\partial r} - \frac{2}{r}\sigma_{r\theta} + \rho g\cos\theta, \end{aligned} \tag{3.19}$$

whose terms scale like

$$0 = (?) - \frac{1}{\mathrm{Re}}\left[\frac{R}{H} + \frac{R}{H}\right] + (?) \tag{3.20}$$

$$0 = (?) - \frac{1}{\mathrm{Re}}\left[\left(\frac{R}{H}\right)^2 + \frac{R}{H}\right] + (?). \tag{3.21}$$

Our plan for the next stage is to take what remains of the $r$-momentum equation, equation (3.18), represented by (3.20), integrate it $\mathrm{d}r$ to find an expression for $p$, and then differentiate it $\mathrm{d}\theta$ to substitute into the $\theta$-momentum equation, equation (3.19), represented by (3.21).

When we integrate equation (3.18) $\mathrm{d}r$, we introduce a scale $H$ into equation (3.20), and so we find that pressure $p$ scales as $\mathrm{Re}^{-1}R$, plus the gravity term. When we differentiate this $\mathrm{d}\theta$ (which offers no scaling) to substitute it into equation (3.19) (at which point we multiply it by $1/r$, introducing a scaling of $1/R$), this term, now of size $\mathrm{Re}^{-1}$, will be dwarfed by the $\mathrm{Re}^{-1}(R/H)^2$ term, so we discard this term in equation (3.18) and so equations (3.18)–(3.19) become

$$0 = -\frac{\partial p}{\partial r} - \rho g\cos\theta \tag{3.22}$$

$$0 = -\frac{1}{r}\frac{\partial p}{\partial\theta} - \frac{\partial\sigma_{r\theta}}{\partial r} + \rho g\sin\theta. \tag{3.23}$$

So, as mentioned already, the approach from here is to integrate equation (3.22) d$r$ to find an equation for $p$, then differentiate it d$\theta$ and substitute that into equation (3.23), which we then try to solve.

Integrating equation (3.22) then gives us

$$p = -\rho g r \cos\theta + p_c,$$

for some constant $p_c$, with the boundary condition at the surface

$$p = p_{\text{atm}} + p_{\text{surf}} \quad \text{at } r = R + h,$$

where $p_{\text{atm}}$ is atmospheric pressure and $p_{\text{surf}}$ is pressure due to surface tension $\gamma_{\text{s}}$, given by the Young–Laplace equation

$$\begin{aligned} p_{\text{surf}} &= -\gamma_{\text{s}} \nabla \cdot \widehat{\mathbf{n}} \\ &\approx -\gamma_{\text{s}} \frac{\partial^2 h}{\partial s^2}, \end{aligned}$$

if the free surface $h$ varies slowly along the coordinate $s$ along the cylinder. Of course, here $s = r\theta$, and so

$$\begin{aligned} &= -\frac{\gamma_{\text{s}}}{r^2} \frac{\partial^2 h}{\partial \theta^2} \\ &= -\frac{\gamma_{\text{s}}}{(R+h)^2} \frac{\partial^2 h}{\partial \theta^2} \end{aligned}$$

on the surface. Hence we are left with an expression for $p$,

$$p = p_{\text{atm}} + \rho g (R + h - r)\cos\theta - \frac{\gamma_{\text{s}}}{(R+h)^2} \frac{\partial^2 h}{\partial \theta^2}. \tag{3.24}$$

Differentiating this d$\theta$,

$$\frac{\partial p}{\partial \theta} = -\rho g (R + h - r)\sin\theta + \rho g \cos\theta \frac{\partial h}{\partial \theta} - \frac{\gamma_{\text{s}}}{(R+h)^2} \frac{\partial^2 h}{\partial \theta^2} + \frac{2\gamma_{\text{s}}}{(R+h)^3} \frac{\partial^2 h}{\partial \theta^2} \frac{\partial h}{\partial \theta}$$

and substituting this into equation (3.23) gives

$$\underbrace{\frac{\partial \sigma_{r\theta}}{\partial r}}_{1} = \underbrace{-\frac{\rho g (R + h - r)\sin\theta}{r}}_{2} + \underbrace{\frac{\rho g \cos\theta}{r} \frac{\partial h}{\partial \theta}}_{3} - \underbrace{\frac{\gamma_{\text{s}}}{r(R+h)^2} \frac{\partial^2 h}{\partial \theta^2}}_{4} + \underbrace{\frac{2\gamma_{\text{s}}}{r(R+h)^3} \frac{\partial^2 h}{\partial \theta^2} \frac{\partial h}{\partial \theta}}_{5} - \underbrace{\rho g \sin\theta}_{6}. \tag{3.25}$$

First comparing the terms with $\rho g$ in them (since we don't know size of $g$), namely terms 2, 3 and 6, we find they scale as

$$\frac{\rho g H}{R}, \qquad \frac{\rho g H}{R}, \qquad \rho g$$

and so clearly term 6 dominates. Comparing the terms without gravity in them, terms 1, 4 and 5, we see they scale as

$$\frac{k}{H}\left(\frac{U}{H}\right)^n, \qquad -\frac{H\gamma_{\text{s}}}{R^3}, \qquad \frac{H^2 \gamma_{\text{s}}}{R^4}. \tag{3.26}$$

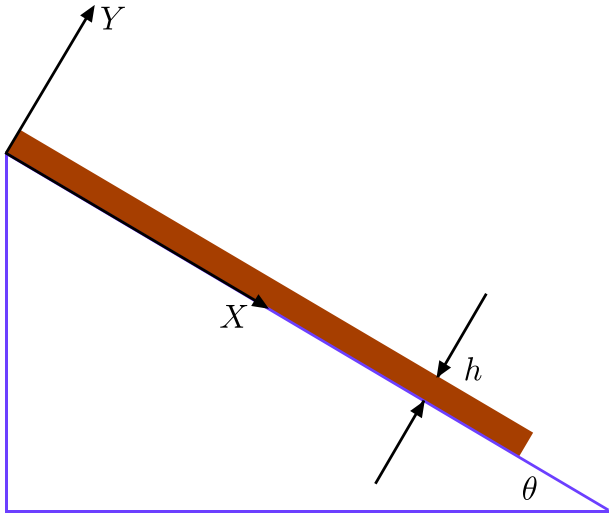


**Figure 3.2:** The velocity profiles we find for the spherical dome, equations (3.34) and (3.33), are equivalent to that we would find for viscous fluid travelling down a flat inclined plane, as shown here.

Of the two terms with $\gamma_s$ in them, $H\gamma_s/R^3$ is clearly bigger. For this term to be the same size as the term on the left-hand side, $k/H(U/H)^n$, this would require

$$\gamma_s \sim \frac{kR^3}{H^2}\left(\frac{U}{H}\right)^n.$$

Using the values from Table 1.1, with our Newtonian data, this would require $\gamma_s \approx 480200\,\mathrm{N\,m^{-1}}$, and with our power-law data, would require $\gamma_s \approx 106705\,\mathrm{N\,m^{-1}}$. In comparison, Table 1.1 tells us that for chocolate, $\gamma_s = 0.0226\,\mathrm{N\,m^{-1}}$, which is considerably smaller! Clearly, then, term 1 in (3.26) dominates over the surface tension terms. So equation (3.25) reduces to

$$\frac{\partial \sigma_{r\theta}}{\partial r} = -\rho g \sin\theta, \tag{3.27}$$

i.e. the viscosity term balances with the gravity term.

At this point we see that the curvature of the problem has disappeared—it's a pure balance of viscosity and gravity. This problem has reduced to what we find for a fluid travelling down an flat inclined plane at an angle $\theta$ to the horizontal, as depicted in Figure 3.2. In other words, the fluid does not experience the curvature of the substrate. Although we have modelled the dome as a hemisphere, we could choose *any* smooth shape for the dome and the velocity profiles we will find shortly would still decribe the flow, given that we know the elevation of the local piece.

This, however, should not be surprising. Our film thickness $h$ changes slowly over the dome, and is tiny compared to the radius of the dome. Furthermore the kind of speeds we expect on the dome are not particularly fast. In fact, we can draw parallels with the shallow water equations from geophysical fluid dynamics, albeit with some Willy Wonka-type chocolatey ocean.

We continue with our analysis, however, by recalling that the stress term $\sigma_{r\theta}$ is given by

$$\sigma_{r\theta} = k\dot{\gamma}^{n-1}\dot{\gamma}_{r\theta}.$$

In equation (3.13), we found that $\dot{\gamma}$ scaled as $U/H$, so to leading order, we take the dominant term in equation (3.12) and find

$$\begin{aligned}\dot{\gamma} &= \left\{\frac{1}{2}\left[r\frac{\partial}{\partial r}\left(\frac{u_r}{r}\right)\right]^2\right\}^{1/2} \\ &= \frac{r}{\sqrt{2}}\frac{\partial}{\partial r}\left(\frac{u_\theta}{r}\right) \\ &= \frac{1}{\sqrt{2}}\left(\frac{\partial u_\theta}{\partial r} - \frac{u_\theta}{r}\right).\end{aligned}$$

The first term here is of order $U/H$, the second is of order $U/R$, which is significantly smaller. So, again, to leading order,

$$\dot{\gamma} = \frac{1}{\sqrt{2}}\frac{\partial u_\theta}{\partial r}. \tag{3.28}$$

Meanwhile, $\dot{\gamma}_{r\theta}$ is given in equation (3.5) as

$$\dot{\gamma}_{r\theta} = \left[r\frac{\partial}{\partial r}\left(\frac{u_\theta}{r}\right) + \frac{1}{r}\frac{\partial u_r}{\partial \theta}\right],$$

which scales as $U/H + V/R$, so the second term is comparatively small (since $U \gg V$ and $H \ll R$), hence we say

$$\begin{aligned}\dot{\gamma}_{r\theta} &= r\frac{\partial}{\partial r}\left(\frac{u_\theta}{r}\right) \\ &= \left(\frac{\partial u_\theta}{\partial r} - \frac{u_\theta}{r}\right) \\ &= \frac{\partial u_\theta}{\partial r}\end{aligned}$$

to leading order, by the same analysis that derived equation (3.28).

So then,

$$\begin{aligned}\sigma_{r\theta} &= k\dot{\gamma}^{n-1}\dot{\gamma}_{r\theta} \\ &= k\left(\frac{1}{\sqrt{2}}\frac{\partial u_\theta}{\partial r}\right)^{n-1}\frac{\partial u_\theta}{\partial r} \\ &= k2^{\frac{1-n}{2}}\left(\frac{\partial u_\theta}{\partial r}\right)^n,\end{aligned}$$

hence

$$\frac{\partial \sigma_{r\theta}}{\partial r} = kn2^{\frac{1-n}{2}}\left(\frac{\partial u_\theta}{\partial r}\right)^{n-1}\frac{\partial^2 u_\theta}{\partial r^2}.$$

So substituting this into equation (3.27), we get

$$kn2^{\frac{1-n}{2}}\left(\frac{\partial u_\theta}{\partial r}\right)^{n-1}\frac{\partial^2 u_\theta}{\partial r^2} = -\rho g\sin\theta,$$

or, rewritten,

$$\frac{\partial^2 u_\theta}{\partial r^2} + \frac{\rho g\sin\theta}{kn2^{\frac{1-n}{2}}}\left(\frac{\partial u_\theta}{\partial r}\right)^{1-n} = 0. \tag{3.29}$$

It is this equation that we want to solve for on the dome, with boundary equations

$$u(R) = 0, \qquad \frac{\partial u}{\partial r}(R+h) = 0,$$

the no-slip condition on the sphere surface and no tangential velocity condition on the fluid surface respectively. We can introduce a shifted coordinate

$$Y = r - R$$

to rewrite equation (3.29) and its boundary conditions as

$$\frac{\partial^2 u_\theta}{\partial Y^2} + \frac{\rho g\sin\theta}{kn2^{\frac{1-n}{2}}}\left(\frac{\partial u_\theta}{\partial Y}\right)^{1-n} = 0. \tag{3.30}$$

with boundary conditions

$$u(0) = 0, \qquad \frac{\partial u}{\partial Y}(h) = 0. \tag{3.31}$$

This equation is too complicated to solve for general $n$, so we look at the two cases we are interested in.

**In the Newtonian case**, $k = \mu$ and $n = 1$ so equation (3.30) becomes

$$\frac{\partial^2 u_\theta}{\partial Y^2} + \frac{\rho g\sin\theta}{\mu} = 0. \tag{3.32}$$

Integrating this with our boundary conditions (3.31) gives

$$u_\theta(Y,\theta) = \frac{\rho g\sin\theta}{2\mu}Y(2h-Y). \tag{3.33}$$

**In the chocolatey power-law case**, we introduce values for our variables from Table 1.1. We round them within experimental error to values which allow an analytical solution (namely, $k = 65, n = 1/3$). Doing so, we look to solve

$$\frac{\partial^2 u_\theta}{\partial Y^2} + 465\sin\theta\left(\frac{\partial u_\theta}{\partial Y}\right)^{2/3} = 0$$

with the boundary conditions (3.31). Doing so gives

$$u_\theta(Y,\theta) = 890000(2h-Y)Y\left(2h^2 - 2hY + Y^2\right)\sin^3\theta. \tag{3.34}$$

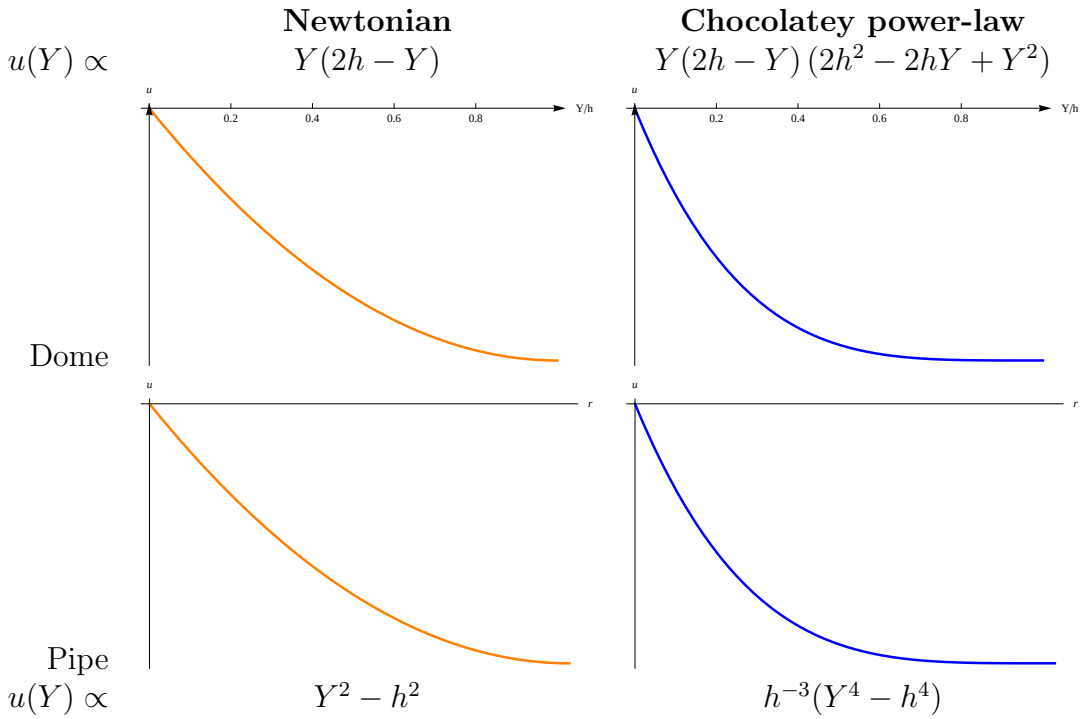


**Figure 3.3:** *Top row*: velocity profiles for the dome, equations (3.33) and (3.34) having fixed $h$ and set $\theta = \pi/2$, i.e. just as as fluid is about to leave the dome. *Bottom row*: velocity profiles of half pipe flow, for a pipe of radius $h$ and radial coordinate $Y$, equations (2.22) and (2.10) respectively. Note how similar the Newtonian profiles (left column) and power-law profiles (right column) are.

Takagi and Huppert (2010) perform this analysis for Newtonian isothermal viscous flows down a cylinder, and find the same velocity profile as we have here. They state that flow down a sphere produces the same velocity profile, which we have shown explicitly.

Having derived these velocity equations, they are, as yet, not in a preferred form since we don't have an easy method of measuring our film thickness $h$ at every point.

If we fix $h$ and $\theta$, we can plot the velocity profiles, as shown in Figure 3.3, where the velocity profiles for half a pipe flow, from the previous chapter, have been added for comparison.

We can overcome the difficulty of measuring $h$ to find our velocities (3.33) and (3.34) by multiplying them by $2\pi Y$ and then integrating them $\mathrm{d}Y$ to find the flux, $Q$. The flux is an experimentally controllable quantity: we know how much chocolate we are pouring into the system, and this is something we can match in the Newtonian and power-law cases to compare the two models.

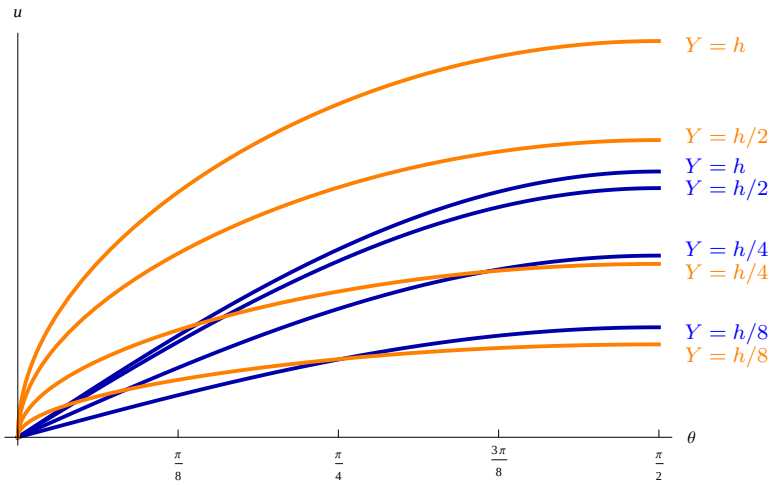


**Figure 3.4:** Velocities following streamlines at different film thicknesses, as functions of $\theta$. Newtonian fluid (equation 3.33) in orange, chocolatey power-law fluid (equation 3.34) in blue. $Q = 4.4 \times 10^{-5}$ as in Figure 3.5, so these velocities relate to that figure.

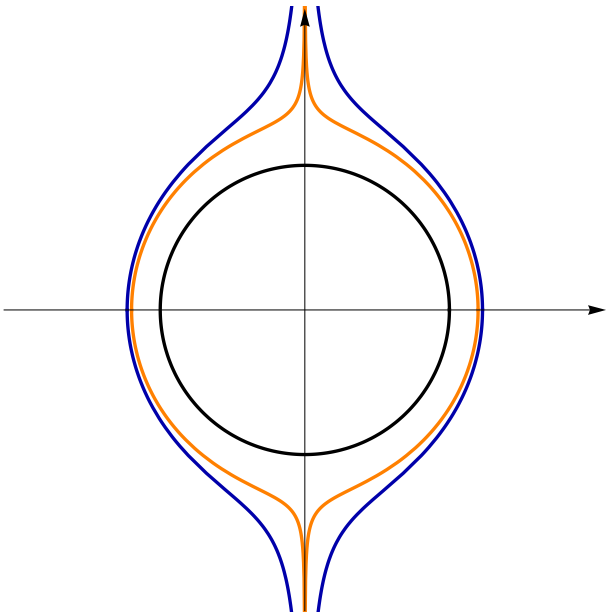

**Figure 3.5:** Flows on the dome in the Newtonian (orange) and power-law (blue) cases respectively. Equation plotted is $r = R + h(\theta)$ for $h$ defined in equations (3.37) and (3.38). $Q = 4.4 \times 10^{-5}\,\mathrm{m^3 s^{-1}}$, a typical flux, and the other values as in Table 1.1. Of course we are only interested in $-\pi/2 \leq \theta \leq \pi/2$.

The fluxes, then, are, for the Newtonian case,

$$Q = \int_0^h 2\pi Y u_\theta(Y)\,\mathrm{d}Y = \frac{5\pi\rho g}{12\mu} h^4 \sin\theta, \tag{3.35}$$

and for the chocolatey power-law case,

$$Q = \int_0^h 2\pi Y u_\theta(Y)\,\mathrm{d}Y = 830000\pi h^6 \sin^3\theta. \tag{3.36}$$

If we fix our flux $Q$, then, we can rearrange these equations to find equations for the film thickness $h(\theta)$: in the Newtonian case,

$$h(\theta) = \left(\frac{12\mu Q}{5\pi\rho g}\right)^{1/4} \sin^{-1/4}\theta, \tag{3.37}$$

and in the chocolatey power-law case,

$$h(\theta) = \frac{Q^{1/6}}{11.73} \sin^{-1/2}\theta. \tag{3.38}$$

These equations have been plotted together for fixed $Q$ in Figure 3.5. We can see that the Newtonian fluid model results in generally thinner films than the chocolatey power law fluid model.

Figure 3.5 is to scale, which is troubling since we do not expect our film flows to be so thick. The global thickness of the film is ultimately governed by $Q$, which we found by estimating the speed of the flow on the dome. If the no-slip condition was not being satisfied on the dome in practice, this would result in higher speeds being observed than our theory predicted, causing us to overestimate $Q$. This is one possible explanation for the excessively thick prediction; of course, our data has come from different sources and so very accurate results are unlikely.

We can also now use these values of $h$ in our equations for $u_\theta$, equations (3.33) and (3.34). These velocities have been plotted as functions of $\theta$ in Figure 3.4, at film thicknesses $h$, $h/2$, $h/4$, $h/8$. What we can see is that Newtonian fluid (in orange) is faster at varying film thicknesses throughout the majority of flow, which matches our observation in the pipe, although close to the surface of the dome, it is slower.

## 3.2 Non-isothermal Newtonian model

In our experiment, the temperature of the chocolate was measured everywhere to be $40 \pm 0.5\,^\circ\mathrm{C}$ (the precision of the thermometer was nearest-degree). Source Wollny (2005) suggests that a change of one degree can cause a 5% to 10% change in viscosity, which is not great in our fountain. However, larger fountains are likely to experience larger changes in temperature and so for completeness we consider a Newtonian fluid with temperature-dependent viscosity,

$$\mu = \mu\big(T(r,\theta)\big).$$

For this section only, we consider working on a cylinder instead of a sphere: the results we find in the 2D case are analogous to the 3D case, but making this simplification allows us to proceed through some unpleasant integration without having to resort to computers. And since we are considering this section for completeness, not for practical prediction, simplifying the geometry seems reasonable.

The analytical work is the same up to equation (3.32) although we are careful with the placement[†] of $\mu$,

$$\frac{\partial}{\partial r}\left(\mu(T(r,\theta))\frac{\partial u}{\partial r}\right) = -\rho g \sin\theta, \tag{3.39}$$

which we solve with the no-slip condition on the surface and vanishing tangential stress on the free surface. However we first scale $r$ by introducing

$$y = \frac{r-R}{h}, \tag{3.40}$$

where $R$ is the radius of the cylinder and $h = h(\theta)$ is the film thickness, so the fluid occupies the space $0 \leq y \leq 1$. This scaling transforms equation (3.39) into

$$\frac{1}{h^2}\frac{\partial}{\partial y}\left(\mu\frac{\partial u}{\partial y}\right) = -\rho g \sin\theta, \tag{3.41}$$

where the partial derivative $\partial/\partial y$ is taken at constant $\theta$, which we want to solve using the initial conditions

$$\begin{aligned} u &= 0 \text{ on } y = 0 \quad \text{(no-slip)} \\ \frac{\partial u}{\partial y} &= 0 \text{ on } y = 1 \quad \text{(kinematic)}. \end{aligned}$$

Doing so gives us the velocity profile

$$u = h^2 \rho g \sin\theta \int_0^y \frac{1-\tilde{y}}{\mu(T(\tilde{y},\theta))}\mathrm{d}\tilde{y}. \tag{3.42}$$

The streamfunction $\psi = \psi(y,\theta)$ in polar coordinates satisfies

$$u = -\frac{\partial \psi}{\partial r} = -\frac{1}{h}\frac{\partial \psi}{\partial y}$$

[†]The Navier–Stokes equation for a general fluid is given in equation (2.11),

$$\rho\frac{\mathrm{D}\mathbf{u}}{\mathrm{D}t} = -\nabla p + \nabla\cdot\boldsymbol{\sigma} + \mathbf{F}.$$

For a Newtonian fluid with viscosity $\mu$, the stress tensor $\boldsymbol{\sigma}$ is given by

$$\sigma_{ij} = \mu\left(\frac{\partial u_i}{\partial x_j} + \frac{\partial u_j}{\partial x_i}\right)$$

where $u_i$ is the velocity in the $i$th direction and $x_j$ is the $j$th direction coordinate. When we take the divergence of $\boldsymbol{\sigma}$ with a non-constant $\mu$, we cannot bring it outside the divergence operator as we have done in (3.32) and so our term remains as (3.39).

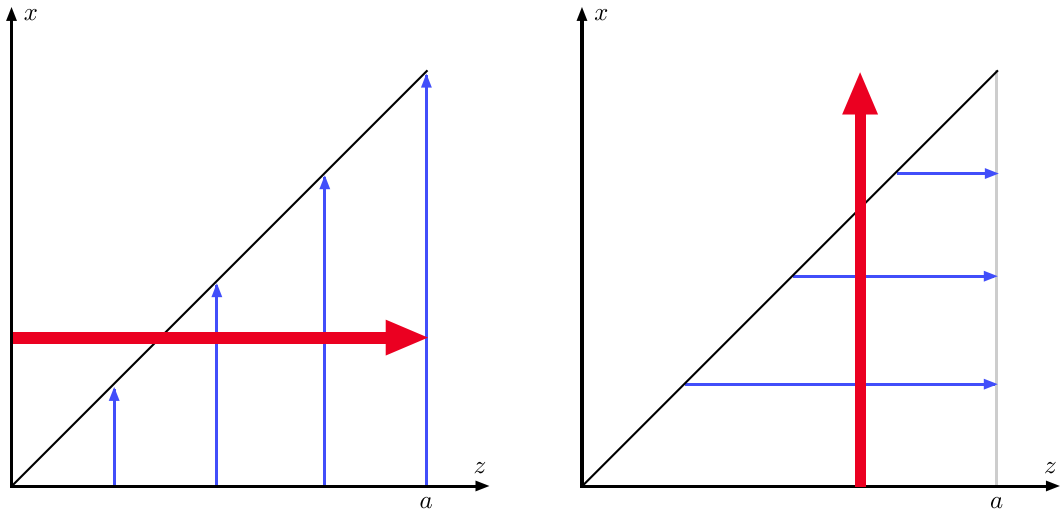


**Figure 3.6:** *Left:* Integrating $\mathrm{d}x$ from 0 to $z$ (thin, blue), and then integrating $\mathrm{d}z$ from 0 to $a$ (thick, red), is equivalent to...
*Right:* Integrating $\mathrm{d}z$ from $x$ to $a$ (thin, blue), and then integrating $\mathrm{d}x$ from 0 to $a$ (thick, red).

and we set $\psi = 0$ on $y = 0$ to give

$$\psi_y = -h^3 \rho g \sin\theta \int_0^y \frac{1-\tilde{y}}{\mu(T(\tilde{y},\theta))} \mathrm{d}\tilde{y} \tag{3.43}$$

$$\begin{aligned} \implies \psi &= -h^3 \rho g \sin\theta \int_0^y \int_0^{\bar{y}} \frac{1-\tilde{y}}{\mu(T(\tilde{y},\theta))} \mathrm{d}\tilde{y}\, \mathrm{d}\bar{y} \\ &= -h^3 \rho g \sin\theta \int_0^y \frac{(1-\tilde{y})(y-\tilde{y})}{\mu(T(\tilde{y},\theta))} \mathrm{d}\tilde{y} \end{aligned} \tag{3.44}$$

where we've used the observation that $\int_0^y \int_0^{\bar{y}} \mathrm{d}\tilde{y}\, \mathrm{d}\bar{y} = \int_0^y \int_{\tilde{y}}^y \mathrm{d}\bar{y}\, \mathrm{d}\tilde{y}$.

[This observation is more obvious if we relabel $y \to a$, $\bar{y} \to z$, $\tilde{y} \to x$. Then I'm claiming that

$$\int_0^a \int_0^z \mathrm{d}x\, \mathrm{d}z = \int_0^a \int_x^a \mathrm{d}z\, \mathrm{d}x.$$

Figure 3.6 demonstrates the validity of this.]

Hence the volume flux $Q = -\psi(1,\theta)$ is given by

$$\begin{aligned} Q &= h^3 \rho g \sin\theta \int_0^1 \frac{(1-\tilde{y})^2}{\mu(T(\tilde{y},\theta))} \mathrm{d}\tilde{y} \\ &= \frac{1}{3} h^3 \rho g \sin\theta \cdot f, \end{aligned} \tag{3.45}$$

where $f = f(\theta)$ represents the fluidity of the fluid film (note this is slightly different from the usual definition of fluidity, $1/\mu$),

$$f = 3 \int_0^1 \frac{(1-y)^2}{\mu(T(y,\theta))} \mathrm{d}y. \tag{3.46}$$

We can see from this form that, if we note that by definition $f \geq 0$ and $h \geq 0$, $Q/\sin\theta \geq 0$, i.e. $Q$ must have the same sign as $\sin\theta$: this is intuitively obvious but Leslie et al. (2011) continue with this argument to show that flow flux behaves like this even when the fluid is not symmetric about the sphere.

This also shows that, given a viscosity model $\mu = \mu(T)$, since the flux $Q$ is prescribed, (3.45) is the equation which determines the film thickness $h$.

We introduce the exponential viscosity model for temperature $T$,

$$\mu(T) = \exp\left(-\frac{\lambda(T - T_0)}{\mu_0}\right) \tag{3.47}$$

which satisfies $\mu = \mu_0, \mathrm{d}\mu/\mathrm{d}T = -\lambda$ for $T = T_0$. The constant $\lambda > 0$ is prescribed and $\mu_0$ is the viscosity of the fluid when $T = T_0$, the uniform temperature of the dome (in the context of the chocolate fountain, we assume that over time the dome warms up to the temperature of the chocolate as it leaves the top of the pipe). We also introduce, as in Leslie et al. (2011), the thermoviscosity number $V$,

$$V = \frac{\lambda(T_0 - T_a)}{\mu_0}, \tag{3.48}$$

where $T_a$ is the ambient (uniform) temperature of the air outside. Since $\mu_0$ and $\lambda$ are both positive, we can use the sign of $V$ to tell which way the temperature gradient goes. High magnitudes of $V$ correspond to fluids whose viscosities depend heavily on temperature, or are being strongly heated/cooled, or both; and low magnitudes of $V$ correspond to fluids whose viscosities are less dependent on temperature, or are being very weakly heated/cooled, or both. For a temperature difference $T_0 - T_a = 25\,^\circ\mathrm{C}$, Balmforth and Craster (2000) give examples of magnitudes: $|V| = 1$ for wax, $|V| = 5$ for basaltic lava and $|V| = 7$ for syrup.

We will be substituting $V$ into equation (3.47) shortly but first we must find an equation that governs the temperature $T$. Temperature following a fluid particle is governed by the heat equation

$$\frac{\mathrm{D}T}{\mathrm{D}t} = c\nabla^2 T,$$

where $c$ is thermal diffusivity, and since we're looking for steady solutions, we look to solve

$$\mathbf{u} \cdot \nabla T = c\nabla^2 T. \tag{3.49}$$

Our boundary conditions are that on the surface of the sphere $y = 0$, $T = T_0$ and on the free surface $y = 1$, we have Newton's law of cooling:

$$-k\nabla T \cdot \widehat{\mathbf{n}} = \alpha(T - T_a), \tag{3.50}$$

where $\alpha$ ($\geq 0$) represents an empirical surface heat-transfer coefficient, $k$ represents the fluid's (constant) thermal conductivity and $\widehat{\mathbf{n}}$ is the unit outward normal.

We now introduce a scaling for $T$, $\mu$, $h$ and $r$ where hats represent the scaled variable:

$$\mu = \mu_0 \widehat{\mu}, \qquad T = T_a + (T_0 - T_a)\widehat{T}. \tag{3.51}$$

If we substitute this scaling into (3.47) and then substitute (3.48) into that we get

$$\widehat{\mu}(\widehat{T}) = \exp(-V(\widehat{T} - 1)). \tag{3.52}$$

We can write our governing equation (3.49) in component $(r, \theta)$ form,

$$\frac{\mathrm{d}r}{\mathrm{d}t}\frac{\partial T}{\partial r} + \frac{\mathrm{d}\theta}{\mathrm{d}t}\frac{\partial T}{\partial \theta} = c\left[\frac{1}{r}\frac{\partial T}{\partial r} + \frac{\partial^2 T}{\partial r^2} + \frac{1}{r^2}\frac{\partial^2 T}{\partial \theta^2}\right]. \tag{3.53}$$

For this argument only, we introduce the scalings from the previous section, equation (3.10),

$$\partial r \sim H, \quad r \sim R,$$

where $H$ is a typical film thickness and $R$ is the radius of the sphere. We also now scale time,

$$t \sim \tau,$$

where $\tau$ is a typical time that the chocolate spends on the dome before falling off. If we now scale equation (3.53) using this scaling as well as that already introduced in (3.51), we get

$$\frac{1}{\tau}\left[\frac{\mathrm{d}\widehat{r}}{\mathrm{d}\widehat{t}}\frac{\partial \widehat{T}}{\partial \widehat{r}} + \frac{\mathrm{d}\theta}{\mathrm{d}\widehat{t}}\frac{\partial \widehat{T}}{\partial \theta}\right] = c\left[\frac{1}{H(H\widehat{r} + R)}\frac{\partial \widehat{T}}{\partial \widehat{r}} + \frac{1}{H^2}\frac{\partial^2 \widehat{T}}{\partial \widehat{r}^2} + \frac{1}{(H\widehat{r} + R)^2}\frac{\partial^2 \widehat{T}}{\partial \theta^2}\right],$$

which scales as

$$\frac{1}{\tau} + \frac{1}{\tau} = c\left[\frac{1}{HR} + \frac{1}{H^2} + \frac{1}{R^2}\right],$$

where we have divided out the temperature scaling. Rearranging, this is equivalent to

$$1 + 1 = \mathrm{Fo}\left[\frac{H}{R} + 1 + \left(\frac{H}{R}\right)^2\right], \tag{3.54}$$

where $\mathrm{Fo} = c\tau/H^2$ is the non-dimensional Fourier number, which measures the ratio of heat conduction rate to the rate of thermal energy storage. Using values for chocolate from Table 1.1 and estimating $\tau = 1\,\mathrm{s}$, we find $\mathrm{Fo} = 0.0632$, which makes the right-hand side of equation (3.53), represented by equation (3.54), comparatively small to the left hand side. In this case, it reduces (3.53) to saying what we already know: the temperature of chocolate does not change while it travels over the fountain. For material comparison, chocolate's thermal diffusivity is given in Table 1.1 as $6.32 \times 10^{-8}\,\mathrm{m^2\,s^{-1}}$. The thermal diffusivity of water at $25\,^{\circ}\mathrm{C}$ is $1.43 \times 10^{-7}\,\mathrm{m^2\,s^{-1}}$ (Blumm and Lindemann, 2003). If we were using water instead of chocolate, with the same film thickness, the time scale $\tau$ would have to be of the order of $10\,\mathrm{s}$ for the Fourier number to be of order 1.

Since we have already established that this section deals with a case that we do not observe on our chocolate fountain, but is nonetheless interesting, we will assume that the Fourier number is of order 10 or higher, allowing the right-hand side to dominate and allowing us to continue.

The dominant term from the right-hand-side of equation (3.53) is the second one (order $\mathrm{Fo}\,/H^2$), so this equation reduces to

$$\frac{\partial^2 \widehat{T}}{\partial \widehat{r}^2} = 0,$$

which is equivalent to

$$\frac{\partial^2 \widehat{T}}{\partial y^2} = 0,$$

since $r = H\widehat{r} + R$ and $r = hy + R$.

We now drop all hats for convenience. We now have to solve, then,

$$\frac{\partial^2 T}{\partial y^2} = 0, \tag{3.55}$$

and our boundary conditions become $y = 0$, $T = 1$ and on the free surface $y = 1$,

$$\begin{aligned} \frac{\partial T}{\partial y} &= -\frac{\alpha H}{k} T \\ &= -BhT \end{aligned} \tag{3.56}$$

where $B = \alpha/k$ is a dimensionalised Biot number (which measures heat transfer at the free surface). We solve this by integrating (3.55) twice, and applying the boundary conditions to find

$$T(y, \theta) = 1 - \frac{Bhy}{1 + Bh}. \tag{3.57}$$

We can now put this form of $T$ into our equation for $\mu$, equation (3.52):

$$\begin{aligned} \mu(T) &= \exp(-V(T-1)) \\ &= \exp\left(\frac{BhVy}{1+Bh}\right) \\ &= \exp(\mathcal{V}y) \end{aligned} \tag{3.58}$$

where for brevity we have followed the convention of Leslie et al. (2011) and used the notation

$$\mathcal{V} = \frac{BhV}{1+Bh}. \tag{3.59}$$

We can now substitute (3.58) into (3.42) to find our velocity profile

$$\begin{aligned} u &= h^2 \rho g \sin\theta \int_0^y (1-\tilde{y}) \exp(-\mathcal{V}\tilde{y})\, \mathrm{d}\tilde{y}. \\ &= \frac{h^2 \rho g \sin\theta}{\mathcal{V}^2} \Big[\mathcal{V} - 1 + \exp(-\mathcal{V}y)[\mathcal{V}(y-1)+1]\Big]. \end{aligned} \tag{3.60}$$

We can also substitute (3.58) into (3.44) to give an expression for the streamfunction

$$\begin{aligned}\psi &= -h^3\rho g\sin\theta\int_0^y(1-\tilde{y})(y-\tilde{y})\exp(-\mathcal{V}\tilde{y})\,\mathrm{d}\tilde{y}\\ &= \frac{-h^3\rho g\sin\theta}{\mathcal{V}^3}\Big[\mathcal{V}^2y-\mathcal{V}(y+1)+2+\exp(-\mathcal{V}y)[\mathcal{V}(1-y)-2]\Big],\end{aligned}\tag{3.61}$$

and into (3.46) to get the fluidity,

$$\begin{aligned}f &= 3\int_0^1(1-y)^2\exp(-\mathcal{V}\tilde{y})\,\mathrm{d}y\\ &= \frac{3}{\mathcal{V}^3}\Big[(\mathcal{V}-1)^2+1-2\exp(-\mathcal{V})\Big].\end{aligned}\tag{3.62}$$

Having found an expression for the fluidity, we can then work out one for $h$ by rearranging (3.45) to get

$$h=\sqrt[3]{\frac{3Q}{f\rho g\sin\theta}},\tag{3.63}$$

although the right-hand side is itself in terms of $h$, since $f=f(\mathcal{V})$ and

$$\mathcal{V}=\frac{BhV}{1+Bh}.$$

Analytic solutions exist for the special case of constant viscosity. If there is no heat transfer to/from the atmosphere at the free surface of the fluid ($\alpha=0$, which in turn means $B=0$), or the viscosity does not depend on temperature ($\lambda=0$ and hence $V=0$) then the fluid has constant viscosity $\mu=1$ and fluidity $f=1$. The latter agrees with asymptotic analysis: observe that (3.62) can be expanded about $V=0$:

$$f=1-\frac{\mathcal{V}}{4}+\frac{\mathcal{V}^2}{20}+O(\mathcal{V}^3)\quad\text{ as }\mathcal{V}\to 0.$$

Of course this then reduces equation (3.63) to the 2D equivalent of (3.37), which has been plotted in Figure 3.5 (in orange). Leslie et al. (2011) have found and plotted numerical solutions for $B,V\neq 0$ (reproduced here in Figure 3.7) and also discuss the cases of $B\to\infty, V\to 0, V\to-\infty$ for further reading.

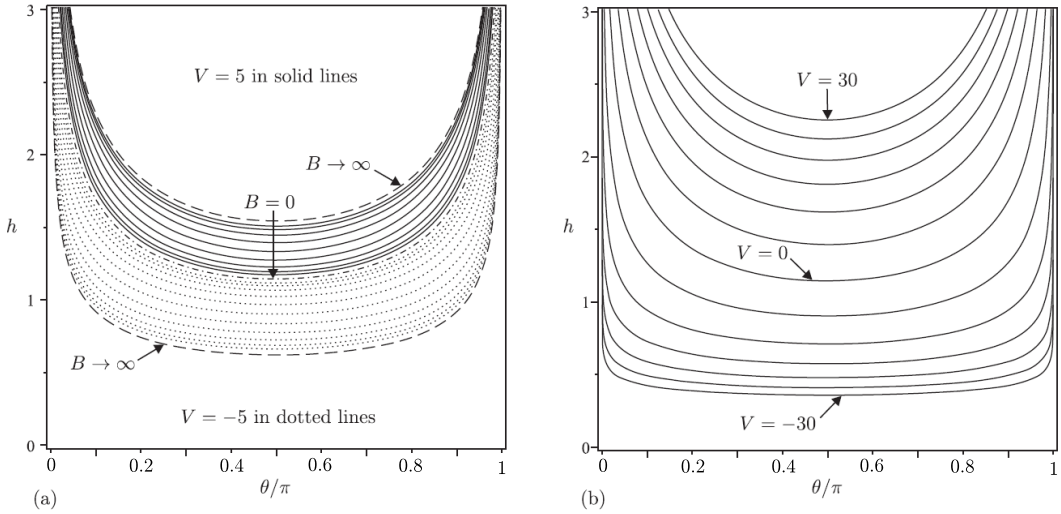


**Figure 3.7:** Film thickness $h$ against $\theta$ for differing values of $B$ and $V$, computed using numerical methods. Source: Leslie et al. (2011)

# Chapter 4

# The falling sheet

Flows in liquid sheets with two free surfaces are considerably harder to describe than film flows over solids with only one free surface. The complication lies in three properties:

1. two free boundaries,
2. the relation between sheet thickness and distance along the sheet is unknown,
3. the position of the sheet's trajectory in space is also unknown.

Flows in sheets are nearly irrotational or extensional since both boundaries of the fluid have no shear upon them, and hence velocity and stress in the streamwise direction does not vary significantly over the sheet cross-section. Viscous effects in the sheet then mainly come from the normal stress difference. We will look for steady flows, but more complications in falling sheets come from their naturally unsteady nature, and how/when they break up.

Furthermore, in our study, the flow is complicated by the shape of the base of the dome, which curves inwards (see Figure 4.11). We will take a look at the different phenomena in effect on the falling sheet.

## 4.1 Inviscid model

Chocolate fountains exhibit behaviour where the falling sheet actually falls *inwards* instead of straight down (see Figure 4.1). Extensive work, starting with Taylor and Howarth (1959), has been conducted on water bells, such as in Figure 4.2, where a jet of water is impacted onto a flat surface (or two jets impacted into each other), and the water spreads out in a thin sheet: essentially it is the water-hitting-a-spoon effect which is undesirable when washing up! Surface tension, as we shall see shortly, then pulls the sheet back inwards to form a closed water bell. We

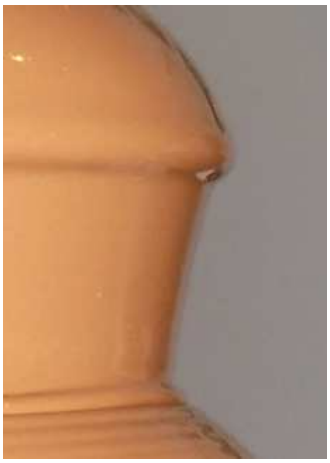

**Figure 4.1:** In the chocolate fountain we can see clearly that the sheet falls inwards once it has left the dome.

are interested in the mathematics of how the surface tension pulls the axisymmetric sheet back in, since this inward-falling effect is observed in our chocolate fountain.

We proceed by constructing a force balance at right-angles to the stream using the method of Button (2005), hence overcoming the first problem by choosing coordinates which follow the falling sheet's path.

We start by setting up the geometry of the falling sheet problem with cylindrical coordinates $(r, \theta, z)$. Since the fluid falls from the dome under gravity, we set our $z$ to be pointing downwards; and we assume the flow to be axisymmetric about the vertical and so consider a 'slice' of the falling sheet in the $(r, z)$ plane, Figure 4.3. We also define local coordinates along and normal to the sheet, $\widehat{\mathbf{s}}, \widehat{\mathbf{n}}$ so that $\mathbf{u} = u\widehat{\mathbf{s}}$. We define the angle $\phi$ to be the small angle between the vertical and the sheet, as shown in Figure 4.3.

We consider a fluid element of length $\mathrm{d}x$, width $\mathrm{d}y$ and thickness $h$, as in Figure 4.4. This element has two principal radii of curvature: the axisymmetric, $R_A$, and the meridian, $R_M$, radii, as shown in Figure 4.5. We assume the element is small enough to approximate the thickness $h$ to be constant within the element. We now consider the forces acting on this element:

1. The force due to gravity acting on the element is
$$\mathbf{F}_{\mathrm{g}} = \rho g h(\cos\phi\,\widehat{\mathbf{s}} + \sin\phi\,\widehat{\mathbf{n}})\mathrm{d}x\mathrm{d}y.$$
2. The pressure force caused by the difference between the internal and external pressures, $\delta p$, is
$$\mathbf{F}_{\mathrm{p}} = -\delta p\,\mathrm{d}x\,\mathrm{d}y\,\widehat{\mathbf{n}}.$$
3. The force due to surface tension is given by
$$\mathbf{F}_{\mathrm{s}} = 2\gamma_{\mathrm{s}}\,\mathrm{d}x\,\mathrm{d}y\left(\frac{1}{R_A} + \frac{1}{R_M}\right)\widehat{\mathbf{n}}.$$

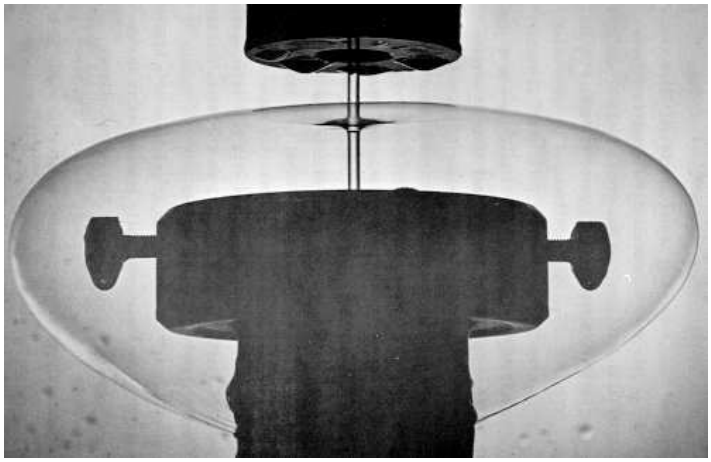

**Figure 4.2:** A water bell in action. Two jets, approximately 3mm in diameter with the top jet slightly larger, collide and form a thin spreading sheet of water. Surface tension pulls the sheet inwards until it forms a closed water bell. Photo by John Huang and John Lienhard; source: Huang and Lienhard (1966).

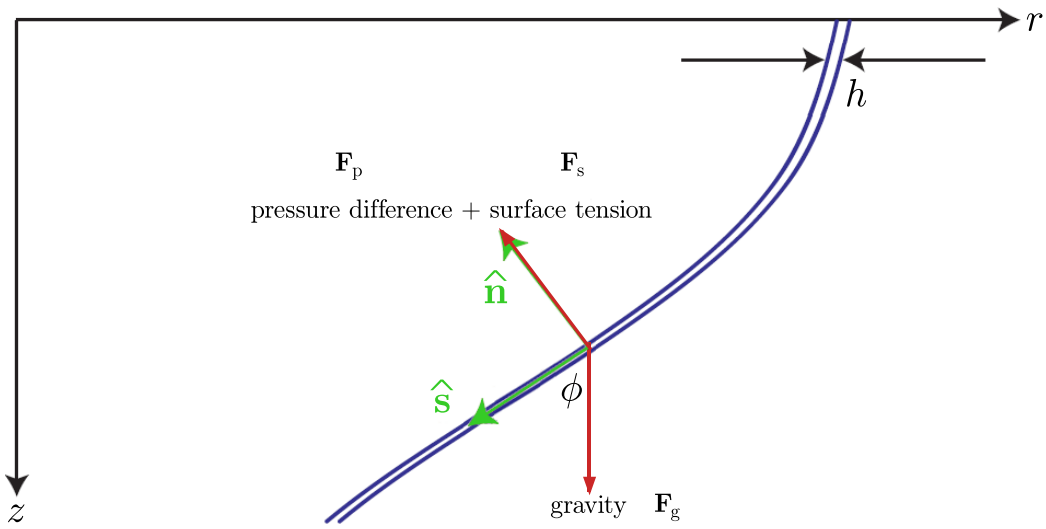


**Figure 4.3:** Setup of the geometry of our problem; adapted from Button (2005).

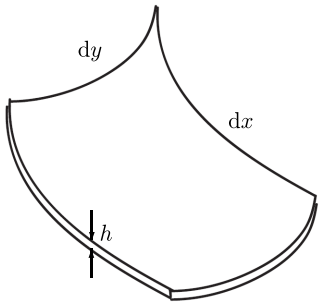


**Figure 4.4:** We consider a fluid element of length $\mathrm{d}x$, width $\mathrm{d}y$ and thickness $h$; adapted from Button (2005).

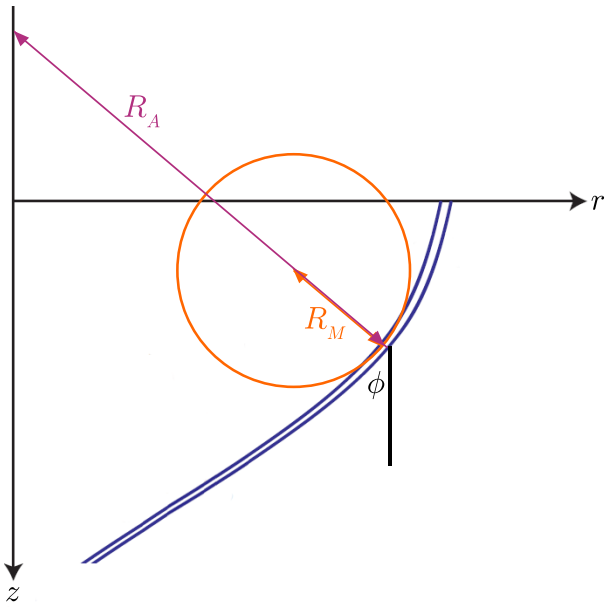


**Figure 4.5:** The fluid element has two principal radii of curvature, $R_A$ and $R_M$. The circle for which $R_A$ is the radius is in the plane normal to the page.

This is since if we take the surface tension $\gamma_s$ to be constant along the surface, then immediately the tangential component of the surface force disappears by symmetry. Noting that there are two surfaces present, the force in the axisymmetric direction of curvature becomes $\frac{2\gamma_s\,\mathrm{d}x\,\mathrm{d}y}{R_A}\widehat{\mathbf{n}}$ and similarly in the meridian direction the force is $\frac{2\gamma_s\,\mathrm{d}x\,\mathrm{d}y}{R_M}\widehat{\mathbf{n}}$. We add these together to give our result above.

We balance these forces by the centripetal acceleration experienced by the fluid particle towards the vertical pipe at any point on the meridian section. This acceleration is $\frac{u^2}{R_M}\widehat{\mathbf{n}}$.

Taking the normal components of the forces and acceleration, and dividing through by $xy$, Newton's second law gives us

$$2\gamma_s\left(\frac{1}{R_A}+\frac{1}{R_M}\right)+\rho gh\sin\phi-\delta p=\frac{\rho hu^2}{R_M} \tag{4.1}$$

where $\rho hxy$ is the mass of the fluid element which appears on the right-hand-side. We now substitute the geometric identities

$$R_A=\frac{r}{\cos\phi}\qquad\frac{1}{R_M}=-\frac{\mathrm{d}\phi}{\mathrm{d}s}$$

into equation (4.1) and we get

$$2\gamma_s\left(\frac{\cos\phi}{r}-\frac{\mathrm{d}\phi}{\mathrm{d}s}\right)+\rho gh\sin\phi-\delta p+\rho hu^2\frac{\mathrm{d}\phi}{\mathrm{d}s}=0. \tag{4.2}$$

We now consider a flow rate argument. Looking down the $z$-axis, cross-sections of the falling sheets are circles of radius $r_{\text{out}}$ and $r_{\text{in}}$. If we say that the position of the

sheet is $r = \frac{1}{2}(r_{\text{out}} - r_{\text{in}})$, then the thickness of the sheet is $h(z) = r_{\text{out}} - r_{\text{in}}$. If the flow rate is constant at $Q$, then by continuity, for all $z$ we have

$$\begin{aligned} Q &= \left[\pi r_{\text{out}}^2(z) - \pi r_{\text{in}}^2(z)\right] u(z) \\ &= 2\pi r h(z) u(z) \\ \implies h(z) &= \frac{Q}{2\pi r u} \end{aligned}$$

Which if we substitute into our value of $h$ in (4.2), we get

$$2\gamma_{\text{s}}\left(\frac{\cos\phi}{r} - \frac{\mathrm{d}\phi}{\mathrm{d}s}\right) + \frac{Q\rho g \sin\phi}{2\pi r u} - \delta p + \frac{\rho Q u^2}{2\pi r u}\frac{\mathrm{d}\phi}{\mathrm{d}s} = 0. \tag{4.3}$$

We now non-dimensionalise our variables by scaling in the following way:

$$\widehat{z} = \frac{z}{L} \quad \widehat{r} = \frac{r}{L} \quad \widehat{s} = \frac{s}{L} \quad \widehat{u} = \frac{u}{u_0}$$

where $u_0$ is our initial velocity as it leaves the dome and

$$L = \frac{\rho Q u_0}{4\pi\gamma_{\text{s}}}.$$

Using values from Table 1.1 and the same flux $Q$ as in Figure 3.5, $L \approx 2\,\text{cm}$, which is roughly how far our fluid falls inwards in experiment, so this is a sensible choice for us to scale our falling sheet on. This scaling in equation (4.3) gives

$$\frac{\cos\phi}{\widehat{r}} - \frac{\mathrm{d}\phi}{\mathrm{d}\widehat{s}} - \alpha + \beta\frac{\sin\phi}{\widehat{u}\widehat{r}} + \frac{\widehat{u}}{\widehat{r}}\frac{\mathrm{d}\phi}{\mathrm{d}\widehat{s}} = 0 \tag{4.4}$$

where

$$\alpha = \frac{\rho Q u_0 \delta p}{8\pi\gamma_{\text{s}}^2} \qquad \beta = \frac{\rho g Q}{4\pi\gamma_{\text{s}} u_0}.$$

We choose this form of the equation since it is clearer than equation (4.4), and hence our falling sheet, only depends on the parameters $\alpha$ and $\beta$. The parameter $\alpha$ accounts for the effect of the inside-outside pressure difference $\delta p$, and $\beta$ accounts for gravity.

We are seeking an equation for $\widehat{r}$ as a function of $\widehat{z}$, $\widehat{r} = \widehat{r}(\widehat{z})$. We now take all variables to be dimensionless as we omit the hats for convenience. Equation (4.4) then becomes

$$\frac{\cos\phi}{r} - \frac{\mathrm{d}\phi}{\mathrm{d}s}\left(\frac{u}{r} - 1\right) - \alpha + \beta\frac{\sin\phi}{ur} = 0 \tag{4.5}$$

which, if we then notice that $r'(z) = \tan\phi$, this gives us

$$\frac{1}{\cos\phi} = \left(1 + r'^2\right)^{1/2} \qquad \frac{\mathrm{d}\phi}{\mathrm{d}s} = r''\cos^3\phi \tag{4.6}$$

and if we substitute this into equation (4.5) we get the final governing equation for the shape of the falling sheet:

$$r''(u - r) + \left(1 + r'^2\right)\left(1 + \frac{\beta}{u}r'\right) - \alpha r\left(1 + r'^2\right)^{3/2} = 0 \tag{4.7}$$

with the initial conditions*

$$r(0) = R/L, \qquad r'(0) = 0 \tag{4.8}$$

Now we want to work out the speed $u$ as a function of $z$ and to do this we need to use the inviscid approximation. We assume that the sheet is thin enough that we can assume to the velocity to be constant through a cross-section at a given $z$. Since the surface of the liquid film is itself a streamline, we can use Bernoulli's (dimensional) equation for any arbitrary point along a streamline where gravity is constant:

$$\frac{1}{2}u^2 - gz + \frac{p}{\rho} = \text{const.}$$

The streamline is also a free surface, so the pressure $p$ is constant, and hence $p/\rho$ is constant. The equation then reduces to

$$u^2 - 2gz = \text{const.}$$

How good this inviscid approximation is, is difficult to determine exactly without being able to measure the speed of the flow reliably throughout its fall. Brunet et al. (2004) use a silicon oil with similar densities and surface tension to chocolate ($\rho = 970\,\mathrm{kg\,m^{-3}}$, $\gamma_\mathrm{s} = 0.0204\,\mathrm{N\,m^{-1}}$) but smaller (but considerably higher than water) viscosity of $0.2\,\mathrm{Pa\,s}$. They were able to measure the speed of the flow as it falls, and plotting the squared speed $u^2$ against $z$, the results were generally along the line $u^2 = 2gz$. Chocolate, of course, is much more viscous, and we will discuss this more later.

Since $u = u_0$ at $z = 0$ when the fluid leaves the dome,

$$u^2 = u_0^2 + 2gz, \tag{4.9}$$

which if we non-dimensionalise as before, becomes

$$u^2 = 1 + 2\beta z. \tag{4.10}$$

We then are left with the complete governing equations (4.7), (4.8) and (4.10) to solve. Analytically this is only possible where $\alpha = \beta = 0$. Although we say later that $\alpha = 0$, since we don't expect any significant pressure difference $\delta p$ between the inside and outside of the sheet, we cannot say this for $\beta$, since this term represents gravity terms, and the Froude number ($U/\sqrt{gR}$), which represents the ratio of inertial to gravitational forces, is order 1. So we will use the scaling arguments given in Button (2005) and reproduced below.

If we take equation (4.2) and substitute the $\phi$ terms for those in equation (4.6) (which come from $Y'(z) = \tan\phi$), we get

$$\frac{2\gamma_\mathrm{s}}{r(1+r'^2)^{1/2}} - \frac{2\gamma_\mathrm{s} r''}{(1+r'^2)^{3/2}} + \frac{\rho g h r'}{(1+r'^2)^{1/2}} - \delta p + \frac{\rho h u^2 r''}{(1+r'^2)^{3/2}} = 0. \tag{4.11}$$

*If we look at Figure 4.1, we can see that the sheet does not fall directly downwards, i.e. $r'(0) < 0$. We could of course measure the angle here and work out which value of $r'(0)$ we want to set as the initial condition, but for sake of argument let's assume ideally that the sheet leaves the dome vertically.

We scale $r$ like $\mathcal{R} = R/L$, the scaled radius of the sphere. Now, in this model, when the fluid leaves the dome, the fluid falls under gravity, and we will assume the flow is dominated by gravity rather than surface tension. If the fluid is left to fall without the presence of either another dome beneath it or the reservoir at the bottom, then the sheet should fall a long distance $\mathcal{Z}$, where $\mathcal{Z} > \mathcal{R}$ but $\mathcal{Z}^2 \gg \mathcal{R}^2$. If we perform scaling analysis on equation (4.11) in this way and then multiply through by $\mathcal{R}$, we find that it scales as

$$\frac{2\gamma_\mathrm{s}}{\left(1+\left(\frac{\mathcal{R}}{\mathcal{Z}}\right)\right)^{1/2}} - \frac{2\gamma_\mathrm{s}\left(\frac{\mathcal{R}}{\mathcal{Z}}\right)^2}{\left(1+\left(\frac{\mathcal{R}}{\mathcal{Z}}\right)^2\right)^{3/2}} + \frac{\rho g h \mathcal{R}\left(\frac{\mathcal{R}}{\mathcal{Z}}\right)}{\left(1+\left(\frac{\mathcal{R}}{\mathcal{Z}}\right)^2\right)^{1/2}} - \delta p\,\mathcal{R} + \frac{\rho h u^2\left(\frac{\mathcal{R}}{\mathcal{Z}}\right)^2}{\left(1+\left(\frac{\mathcal{R}}{\mathcal{Z}}\right)^2\right)^{3/2}} \sim 0.$$

Since $(\mathcal{R}/\mathcal{Z})^2 \ll 1$, this equation, where we have divided through by $\mathcal{R}$, reduces to

$$\frac{2\gamma_\mathrm{s}}{\mathcal{R}} + \frac{\rho g h \mathcal{R}}{\mathcal{Z}} - \delta p \sim 0,$$

which represents

$$\frac{1}{r} + \beta\frac{r'}{r} - \alpha = 0$$

from equation (4.11).

We now argue that the pressure difference between the inside and the outside of the sheet is zero, since the sheet in reality is not continuous enough to form a proper seal. So $\alpha = 0$ and hence equation (4.11) reduces to

$$r'(z) = -\frac{u}{\beta}, \tag{4.12}$$

and substituting in equation (4.10),

$$r'(z) = -\frac{(1+2\beta z)^{1/2}}{\beta}.$$

Which, when integrated with the boundary condition $r(0) = R/L$ (remember $z$ has been scaled here), produces an equation for $r$,

$$r(z) = \frac{R}{L} + \frac{1-(1+2\beta z)^{3/2}}{3\beta^2}. \tag{4.13}$$

This equation (in dimensional form) has been plotted in Figure 4.6, with data from Table 1.1. We can see that it captures the essence of what we see in the falling sheet, photographed in Figure 4.1, and shows the sheet falling inwards due to surface tension with slope of the same order we expect. However, this model does not match in all the right places. Firstly, it predicts that the sheet falls in about 3 cm over the 7 cm drop, when we observe in experiment only about half that. Secondly, we can see in Figure 4.1 that the falling sheet does not start by falling directly down—it falls from the beginning at a slant, and we have lost the ability to set $r'(0)$ in doing this scaling analysis which reduces the order of the governing equation. We will shortly go on to explain the other effects at work here.

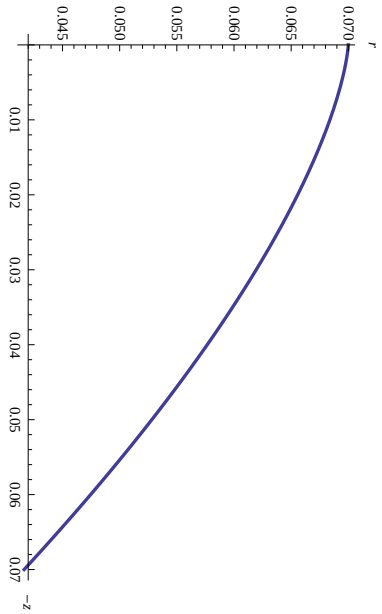


**Figure 4.6:** Plot of the dimensionalised form of equation (4.13) with values from Table 1.1. We can see that this produces a shape which captures of the essence of what we see, but falls too far inwards.

### 4.1.1 Validity of inviscid approximation

Viscous effects are expected to play a part here, as shown by the following calculation. We will compare the energy used in the work done by viscous forces in the falling fluid, $K$, with the total energy coming in from the previous stage, $E$, and show that viscous effects should be apparent in our analysis of the falling sheet.

Cauchy's energy equation for energy $K$ in a viscous Newtonian fluid of volume $V$ and viscosity $\mu$ is, generally,

$$\frac{\mathrm{d}K}{\mathrm{d}t} = -\int_V 2\mu\dot{\gamma}_{ij}\dot{\gamma}_{ij}\,\mathrm{d}V \tag{4.14}$$

where $\dot{\gamma}_{ij}$ is the $ij$th component of our rate of strain tensor $\dot{\boldsymbol{\gamma}}$. But

$$\dot{\gamma}_{ij} = \frac{1}{2}\left(\frac{\partial u_i}{\partial x_j} + \frac{\partial u_j}{\partial x_i}\right) \tag{4.15}$$

in coordinates $(x_1, x_2, x_3)$ with respective velocities $(u_1, u_2, u_3)$.

We have worked out from our geometry in equation (4.9) that, in dimensionalised form,

$$u^2 = u_0^2 + 2gz$$

in $\mathrm{m\,s^{-1}}$. Hence

$$\frac{\mathrm{d}u}{\mathrm{d}z} = \frac{g}{(u_0^2 + 2gz)^{1/2}} \tag{4.16}$$

in $\mathrm{s}^{-1}$. Now the velocity is predominantly vertical, and so we say that the dominant rate of strain tensor is $\dot{\gamma}_{33}$, if we briefly use Cartesian coordinates $(x, y, z)$ with an inverted $z$ component. Hence, plugging equation (4.16) into equation (4.15) we get

$$\dot{\gamma}_{33} = \frac{g}{(u_0^2 + 2gz)^{1/2}}$$

in $\mathrm{s}^{-1}$. Now the fluid is incompressible ($\nabla \cdot u = 0$) and so $\dot{\boldsymbol{\gamma}}$ is traceless ($\sum_i \dot{\gamma}_{ii} = 0$). Hence at best, $\dot{\gamma}_{11} = \dot{\gamma}_{22} = -\frac{1}{2}\dot{\gamma}_{33}$ or at worst, $\dot{\gamma}_{11} = -\dot{\gamma}_{33}$ and $\dot{\gamma}_{22} = 0$. Taking the best-case scenario and substituting into equation (4.14) we get

$$\begin{aligned}
\frac{\mathrm{d}K}{\mathrm{d}t} &= -\int_V 3\mu \frac{g^2}{u_0^2 + 2gz}\,\mathrm{d}V \\
&= -3\mu g^2 \int_V \frac{1}{u_0^2 + 2gz}\,\mathrm{d}z \cdot xy \\
&= -\frac{3}{2}\mu g \left[\log(2gz + u_0^2)\right]_0^\ell \cdot xy \\
&= -\frac{3}{2}\mu g \log\left(\frac{2g\ell}{u_0^2} + 1\right) \cdot xy
\end{aligned} \tag{4.17}$$

in $\mathrm{J\,s}^{-1}$, where $xy$ is $\int \mathrm{d}x\,\mathrm{d}y$ and $\ell$ is the height of the drop.

Compare this to the kinetic energy $E_K$ entering the system

$$\begin{aligned}
E_K &= \frac{1}{2}\rho \int_V u^2\,\mathrm{d}V \\
&= \frac{1}{2}\rho \int_0^\ell \left(u_0^2 + 2gz\right)\mathrm{d}z \cdot xy \\
&= \frac{1}{2}\rho \left(u_0^2\ell + g\ell^2\right) \cdot xy
\end{aligned}$$

in Joules, and the potential energy difference $E_P$ of the system at the top and bottom

$$\begin{aligned}
E_P &= \int_0^\ell \rho g z\,\mathrm{d}z \cdot xy \\
&= \rho g \frac{\ell^2}{2} \cdot xy
\end{aligned}$$

also in Joules.

Substituting our values from Table 1.1 into these equations, we find that in a fifth of a second, an estimate for how long it takes chocolate to complete its fall, the energy absorbed by viscous forces $K$ is equal to $208xy\,\mathrm{J}$. The combined kinetic and potential energy entering the sheet from the dome is $E = E_K + E_P = 101xy\,\mathrm{J}$. So we see that the viscous forces are expected to contribute highly.

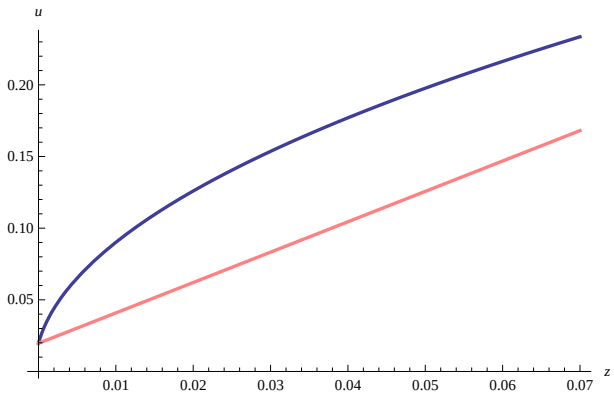


**Figure 4.7:** Plot of dimensionalised velocity of the sheet as a function of $z$ in the inviscid (blue, equation 4.10) and viscous (pink, equation 4.18, $\mu = 10\,\mathrm{Pa\,s}$) cases.

## 4.2 Viscous model

Gilio et al. (2005) examine 2D falling nonsteady liquid sheets, deriving governing equations through a different (and newer, but less intuitive) method, and discusses viscous effects at the end. The viscous equations are solved numerically using finite-difference methods, and the results are interesting and relevant to our falling sheet of chocolate.

Figure 4.7 plots the velocity of the sheet as a function of $z$ in the inviscid and viscous cases. The inviscid plot is equation (4.10), derived by us. Gilio et al. (2005) give results for both their inviscid and viscous (where they have used a fluid with viscosity $10\,\mathrm{Pa\,s}$, close to our chocolate value of $14\,\mathrm{Pa\,s}$) cases, and we have matched our inviscid graph with theirs to find the equation governing the viscous velocity, which is remarkably linear and is given in non-dimensional form by

$$u(z) = 1 + 2.12z. \tag{4.18}$$

We can substitute this velocity into equation (4.12) to find an equation governing the position of the viscous sheet in time, namely

$$r(z) = \frac{R}{L} - \frac{z + 1.06z^2}{\beta}, \tag{4.19}$$

recalling that these equations are still nondimensional. This has been plotted (in dimensional form) in Figure 4.8, alongside the inviscid case for comparison. What we see in this plot is that the viscous sheet does not fall as far inwards as in the inviscid prediction, instead only falling about $1.5\,\mathrm{cm}$ inwards over the $7\,\mathrm{cm}$ drop: this very closely matches what we observe in running the chocolate fountain.

Figure 4.9 shows the profile of the falling sheets in the inviscid and viscous cases for artificially lower and higher surface tensions than that given (and used in Figure 4.8) for chocolate. Predictably, higher surface tensions bring the sheet in further. Interestingly, it affects the viscous sheet more than the inviscid sheet, with the

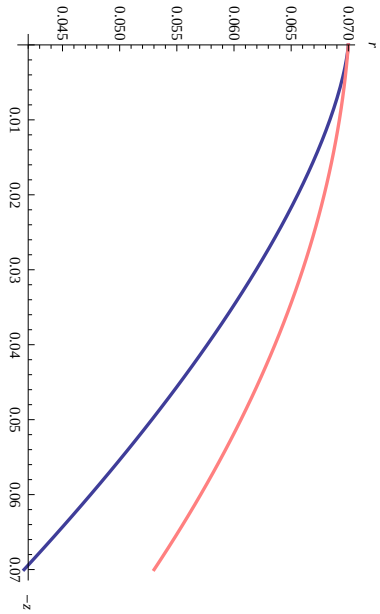


**Figure 4.8:** Profile of the falling sheet from the equations derived in the inviscid (blue, equation 4.13) and viscous (pink, equation 4.19, $\mu = 10\,\mathrm{Pa\,s}$) cases. The inviscid case is the same as Figure 4.6, and the viscous case has been matched from the results in Gilio et al. (2005).

viscous sheet falling further inwards in the higher surface tension case than the inviscid prediction.

## 4.3 The teapot effect

The so-called 'teapot effect' was first written about in Reiner (1956), where the term was coined. The effect is an everyday occurrence and is shown in Figure 4.10: when pouring tea from a teapot at fairly slow speeds, the tea has a tendency to curve backwards and dribble down the spout instead of falling nicely into the cup. The relevance to our chocolate fountain problem is that, as shown in Figure 4.11, the dome from which the chocolate falls is curved at the edge, which is a property of badly-formed teapots. Of course, in teapots, this falling backwards is not a phenomenon that we want, although in a chocolate fountain, we do want this because it produces the aesthetic of the inward-falling sheet. Considerable work has been done on the teapot effect, summarised nicely in the introduction of Kistler and Scriven (1994), and here we discuss just a few of the explanations.

The analogy is not full, though, since we have no spout and the dome is hollow. The teapot effect is not 3D and axisymmetric, however, Kistler (1983) derives governing equations for an axisymmetric viscous falling sheet in the same manner as the 2D 'teapot' case. The physics responsible for the teapot effect is however relevant to both the teapot and our fountain, so we shall entertain the teapot effect for a few paragraphs.

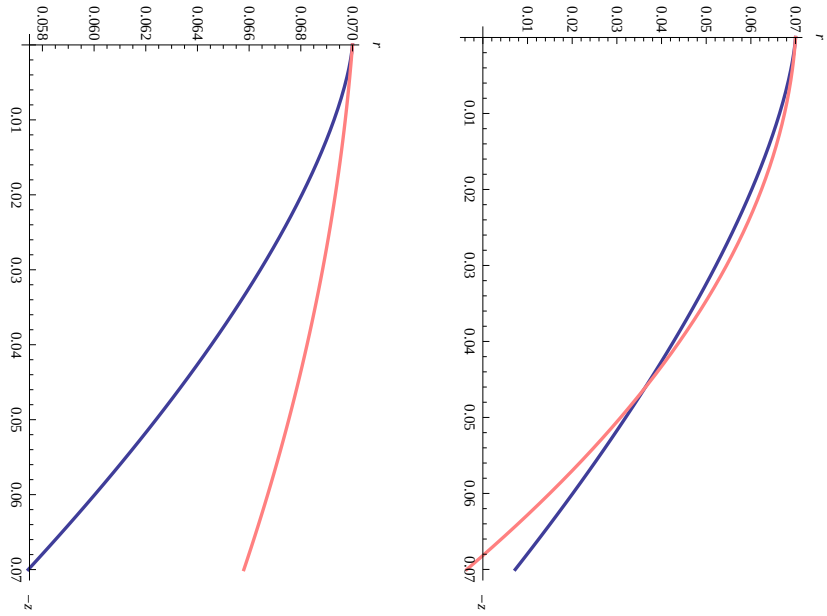


**Figure 4.9:** Profile of the falling sheets in the inviscid (blue) and viscous (pink) cases, with different surface tensions. *Left*: $\gamma_s = 0.01\,\mathrm{N\,m^{-1}}$. *Right*: $\gamma_s = 0.05\,\mathrm{N\,m^{-1}}$. The surface tension of chocolate, used in Figure 4.8 is $0.0226\,\mathrm{N\,m^{-1}}$.

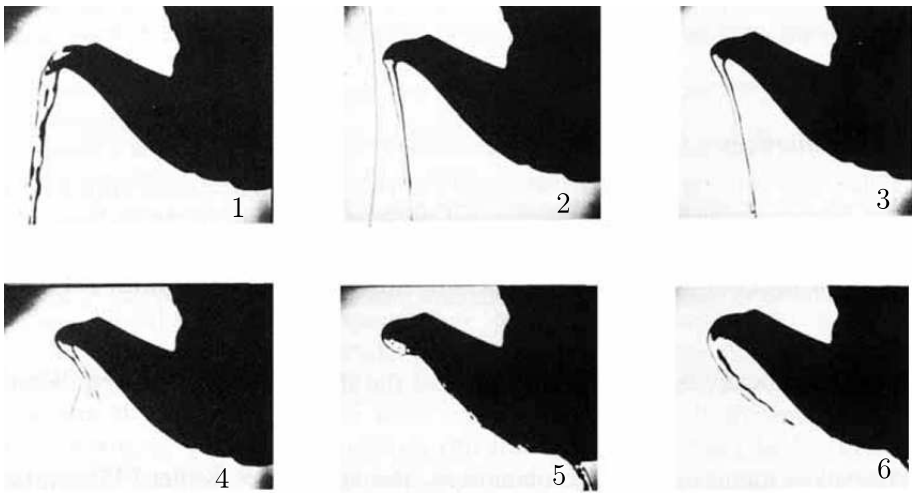


**Figure 4.10:** The teapot effect in action. Tea is poured from the spout at decreasing velocities in images 1–5, and the tea deflects backwards towards the spout. Flow is increased again in image 6, and we can see an even stronger effect. Source: Kistler and Scriven (1994).

**Figure 4.11:** Relevance of the teapot effect to our chocolate fountain. The edge of the dome, from which the chocolate falls, is curved, emphasised by the arrow.

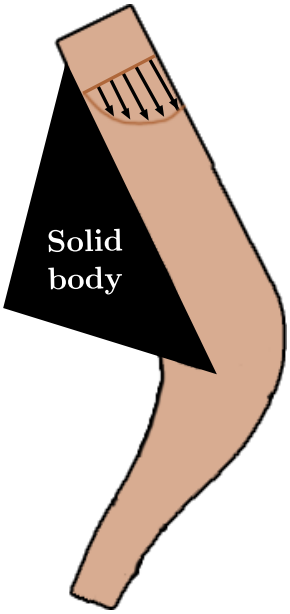


**Figure 4.12:** What we see when we pour liquid down a slope is that the liquid creeps upwards instead of falling entirely downwards. This contributes to an inwards-falling sheet. Adapted from Kistler and Scriven (1994).

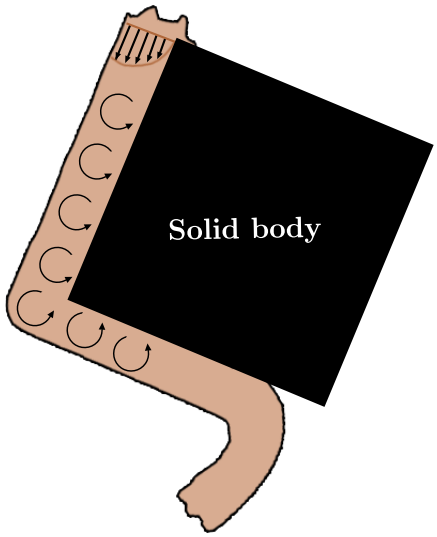


**Figure 4.13:** Reiner's first hypothesis for the teapot effect. 'Vortices' are created along the fluid path due to the velocity profile, which pushes the fluid towards the underside of the body it is flowing around. Adapted from Reiner (1956).

Figure 4.12 shows diagrammatically what we see when we pour liquid down a slope before it falls off: the fluid creeps upwards before falling down. Surface tension is responsible, as we saw in Section 4.1, for the sheet falling inwards. However, it is not, as Reiner writes, surface tension which is responsible for this creep effect.

Reiner makes two observations about the fluid continuing to move backwards, the first of which he offers an explanation for, which we will mention. Figure 4.13 shows this: that 'vortices' are created along the fluid path due to the velocity profile, which pushes the fluid towards the underside of the body as it flows around.

Keller (1957) gives a different explanation, quoted here:

> *Qualitatively the explanation is this. When the liquid flows around the lip its velocity is greatest at the lip. By Bernoulli's principle the pressure is then lowest there. Consequently the surrounding air or other fluid pushes the liquid against the lip by virtue of its atmospheric pressure. This enables the flow to turn the corner. Once the flow has turned the corner it continues along the underside of the spout rather than falling because the surrounding air supports it. This upside-down flow, although unstable, will travel quite far down the spout before its instability results in detachment, if the liquid layer is thin. When detachment occurs the jet will fall backwards since its velocity is directed away from the lip.*

This explanation is supported with mathematical work considering 2D flow of inviscid, incompressible fluid leaving a horizontal spout. Once again, we see that the viscosity of the fluid is not a cause of deflection in the flow.

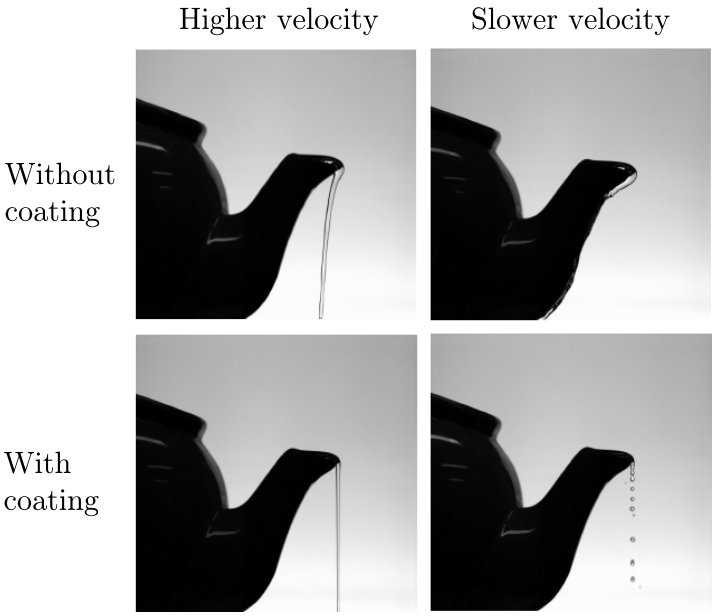


**Figure 4.14:** Applying a super-hydrophobic coating to the spout reduces the teapot effect in experiment. Source: Duez et al. (2009).

Duez et al. (2009) argue that surface wettability is an important factor, following experiment. They argue that coating the spout of the teapot with a super-hydrophobic surface avoids the teapot effect altogether, as shown in Figure 4.14. Of course, in the chocolate fountain, this could be useful information: to maximise the teapot effect to produce inwards-falling sheets, one should wet the undersides of the domes first. This conclusion seems to contradict that of Reiner, who says that coating the spout with some water-repelling material didn't make any difference, hence suggesting that surface tension plays very little part in the dynamics of the fluid. It cannot be argued that such super-hydrophobic materials as used by Duez et al. were not invented: in Figure 4.14 they have coated the teapots with black soot, which would have been more prevalent in the time of Reiner.

Ultimately the teapot effect is a complicated phenomenon which is, due to time, beyond the scope of this project to investigate fully. I have only briefly discussed the physics behind various studies but more rigorous and full analysis could be a project of its own, particularly since it involves considerable numerical work.

## 4.4 Concluding remarks on the falling sheet

The falling sheet is a difficult problem because there are a number of different phenomena acting together. The teapot effect showcases some of these quite nicely. We were able to solve for an inviscid falling sheet by simplifying the problem, but viscous falling sheets require numerical work which, due to time constraints, we have not been able to undertake. Relevant published papers that have performed this work have been mentioned.

# Bibliography

J.-M. Aeschlimann and S. T. Beckett. International interlaboratory trials to determine the factors affecting the measurement of chocolate viscosity. *Journal of Texture Studies*, 31(5):541–576, November 2000. ISSN 1745-4603. doi: 10.1111/j.1745-4603.2000.tb01019.x. URL `http://onlinelibrary.wiley.com/doi/10.1111/j.1745-4603.2000.tb01019.x/abstract`.

Emmanuel Ohene Afoakwa, Alistair Paterson, Mark Fowler, and Joselio Vieira. Comparison of rheological models for determining dark chocolate viscosity. *International Journal of Food Science & Technology*, 44(1):162–167, January 2009. ISSN 09505423, 13652621. doi: 10.1111/j.1365-2621.2008.01710.x. URL `http://strathprints.strath.ac.uk/16013/`.

N. J. Balmforth and R. V. Craster. Dynamics of cooling domes of viscoplastic fluid. *Journal of Fluid Mechanics*, 422:225–248, November 2000. ISSN 00221120. URL `http://resolver.scholarsportal.info/resolve/00221120/v422inone/225_docdovf.xml`.

Jrgen Blumm and Andr Lindemann. Characterization of the thermophysical properties of molten polymers and liquids using the flash technique. *High Temperatures - High Pressures*, 35/36(6):627–632, 2003. doi: 10.1068/htjr144. URL `http://thermophysics.ru/pdf_doc/AutoPlay/Docs/CollectionOfManuscripts/ECTP2005paper104.pdf`.

P. Brunet, C. Clanet, and L. Limat. Transonic liquid bells. *Physics of Fluids*, 16 (7):2668, 2004. ISSN 10706631. doi: 10.1063/1.1738650. URL `http://link.aip.org/link/PHFLE6/v16/i7/p2668/s1&Agg=doi`.

Eleanor C. Button. *The dynamics of water bells*. Honours thesis, University of Melbourne, Mathematics & Statistics, November 2005. URL `http://www.ms.unimelb.edu.au/publications/button.pdf`.

N. Casson. A flow equation for pigment-oil suspensions of the printing ink type. In C. C. Mill, editor, *Rheology of disperse systems: Proceedings of a conference organized by the British Society of Rheology and held at the University College of Swansea in September 1957*. Pergamon Press, 1959.

C. R. Daubert, J. F. Steffe, and J. R. Lloyd. Electric field effects on the thermal conductivity of milk chocolate determined using the mirror image method. *Journal*

*of Food Process Engineering*, 20(1):77–89, February 1997. ISSN 1745-4530. doi: 10.1111/j.1745-4530.1997.tb00412.x. URL http://onlinelibrary.wiley.com.libproxy.ucl.ac.uk/doi/10.1111/j.1745-4530.1997.tb00412.x/abstract.

C. Duez, C. Ybert, C. Clanet, and L. Bocquet. Beating the teapot effect. *Physical Review Letters*, 104:084503, October 2009. URL http://arxiv.org/abs/0910.3306.

M. Gilio, F. Al-Bender, and J.-P. Kruth. The dynamics of a moving sheet of liquid, part I: derivation of the 2D equations of motion. *European Journal of Mechanics - B/Fluids*, 24(5):555–571, October 2005. ISSN 0997-7546. doi: 10.1016/j.euromechflu.2004.12.003. URL http://www.sciencedirect.com/science/article/pii/S0997754604001311.

C. P. Huang and J. H. Lienhard. The influence of gravity upon the shape of water bells. *Journal of Applied Mechanics*, 33(2):457, 1966. ISSN 00218936. doi: 10.1115/1.3625072. URL http://adsabs.harvard.edu/abs/1966JAM....33..457H.

Esther L. Keijbets, Jianshe Chen, Eric Dickinson, and Joselio Vieira. Surface energy investigation of chocolate adhesion to solid mould materials. *Journal of Food Engineering*, 92(2):217–225, May 2009. ISSN 0260-8774. doi: 10.1016/j.jfoodeng.2008.11.008. URL http://www.sciencedirect.com/science/article/pii/S026087740800544X.

Joseph B. Keller. Teapot effect. *Journal of Applied Physics*, 28(8):859–864, August 1957. ISSN 00218979. doi: 10.1063/1.1722875. URL http://jap.aip.org.libproxy.ucl.ac.uk/resource/1/japiau/v28/i8/p859_s1.

S. F. Kistler and L. E. Scriven. The teapot effect: sheet-forming flows with deflection, wetting and hysteresis. *Journal of Fluid Mechanics*, 263:19–62, 1994. doi: 10.1017/S0022112094004027.

Stephan F. Kistler. *The fluid mechanics of curtain coating and related viscous free surface flows with contact lines*. PhD thesis, University of Minnesota, November 1983.

G. A. Leslie, S. K. Wilson, and B. R. Duffy. Non-isothermal flow of a thin film of fluid with temperature-dependent viscosity on a stationary horizontal cylinder. *Physics of Fluids*, 23(6):062101, 2011. ISSN 10706631. doi: 10.1063/1.3593393. URL http://strathprints.strath.ac.uk/33826/.

Gagan Mongia and Gregory R. Ziegler. The role of particle size distribution of suspended solids in defining the flow properties of milk chocolate. *International Journal of Food Properties*, 3(1):137–147, 2000. ISSN 1094-2912. doi: 10.1080/10942910009524621. URL http://www.tandfonline.com.libproxy.ucl.ac.uk/doi/abs/10.1080/10942910009524621.

Savina Radosasvljevic, Anna Schlunk, Roger Tanner, and Simin Nasseri. Melting chocolate, February 2000. URL `http://web.aeromech.usyd.edu.au/rheology/snasseri/images/chocolate.pdf`.

Markus Reiner. The teapot effect... a problem. *Physics Today*, 9(9):16, 1956. ISSN 00319228. doi: 10.1063/1.3060089. URL `http://www.physicstoday.org/resource/1/phtoad/v9/i9/p16_s1?isAuthorized=no`.

Serpil Sahin and Servit Gulum Sumnu. *Physical properties of foods*. Springer, 2006. ISBN 9780387307800.

Daisuke Takagi and Herbert E. Huppert. Flow and instability of thin films on a cylinder and sphere. *Journal of Fluid Mechanics*, 647: 221, March 2010. ISSN 0022-1120, 1469-7645. doi: 10.1017/S0022112009993818. URL `http://65.54.113.26/Publication/26707321/flow-and-instability-of-thin-films-on-a-cylinder-and-sphere`.

Geoffrey Taylor and L. Howarth. The dynamics of thin sheets of fluid. I. Water bells. *Proceedings of the Royal Society of London. Series A. Mathematical and Physical Sciences*, 253(1274):289 –295, December 1959. doi: 10.1098/rspa.1959.0194. URL `http://rspa.royalsocietypublishing.org/content/253/1274/289.abstract`.

Sukanya Wichchukit, Michael J. McCarthy, and Kathryn L. McCarthy. Flow behavior of milk chocolate melt and the application to coating flow. *Journal of Food Science*, 70(3):E165–E171, April 2005. ISSN 1750-3841. doi: 10.1111/j.1365-2621.2005.tb07131.x. URL `http://onlinelibrary.wiley.com.libproxy.ucl.ac.uk/doi/10.1111/j.1365-2621.2005.tb07131.x/abstract`.

William Lionel Wilkinson. *Non-Newtonian fluids: fluid mechanics, mixing and heat transfer*. Pergamon Press, 1960.

Klaus Wollny. Determining the yield point and viscosity of chocolate, February 2005. URL `http://www.mep.net.au/foodlab/FL_7/AN_RLQC_Choco_B.pdf`.